Vibrational properties of amorphous Si and Ge†

R. Alben and D. Weaire
Department of Engineering and Applied Science, Yale University, New Haven, Connecticut 06520

J. E. Smith, Jr. and M. H. Brodsky
IBM Thomas J. Watson Research Center, Yorktown Heights, New York 10598

(Received 10 September 1974)

Calculations of the vibrational density of states and the Raman and infrared spectra have been performed for random-network, microcrystalline, and polymorph structures of Si and Ge. The polymorphs considered include Si III, Ge III, and two clathrate structures. The calculations are based on simple semiempirical forms for interatomic interactions and Raman and infrared activities. The results for some representations of the random network compare favorably with experimental measurements on amorphous Si and Ge. The apparent similarity of the vibrational densities of states of amorphous Si and Ge to those of diamond cubic Si and Ge is explained by a study of the form of the density of states for nearest-neighbor central forces. There is an interesting relationship to a simple tight-binding theory of the electronic density of states in this limit. The variations of infrared and Raman activities in different parts of the spectrum are discussed. Numerical calculations for energy-loss spectra in neutron scattering are also presented. A simple model explains the oscillation of intensity between the high- and low-frequency parts of the spectrum as the scattering vector increases.

I. INTRODUCTION

In this paper we gather together the available experimental data on the vibrational properties of amorphous Si and Ge and present a theoretical analysis of most of the major features of the observations as well as some predictions for neutron scattering. The theory is of a semiempirical nature. It would clearly be most inappropriate to attempt for amorphous semiconductors what is already a difficult undertaking for their crystalline counterparts, namely, the calculation from first principles of vibrational eigenstates, band structure, and hence the Raman and infrared cross sections which depend upon them. We choose instead to use a simple force-constant prescription for the calculation of the vibrational spectrum and express the matrix elements for Raman and infrared intensities in terms of contributions from individual bonds, involving few adjustable parameters.

In addition to such a scheme for the calculation of spectra, one must adopt a specific model for the structure of amorphous Si and Ge. Indeed, current uncertainties regarding the details of this structure provided much of the motivation for this study, since it was hoped that vibrational properties might offer a further means of discriminating between rival structural models. All that is reasonably certain, on the basis of x-ray diffraction evidence,[1] is that amorphous Si and Ge are tetrahedrally bonded, with bond lengths equal to those of their crystalline forms to within about 1% and a modest spread of bond angles about the ideal value of the order of ten deg. Beyond this, one can only say that the diffraction data are persuasive of the validity of the random-network model of Polk[2] and others, but not conclusive. In particular, Rudee and Howie[3] have suggested on the basis of other evidence that the structure of amorphous Si and Ge is of a microcrystalline nature, the microcrystals being of the wurtzite structure, and they claim such a model can be compatible with the x-ray data.

In most of our calculations we employ representations of the continuous-random-network structure. Since there is no unique set of coordinates which defines such a structure, we have done calculations on a number of network models, including those of Henderson[4] and Polk,[2] as well as models which we ourselves have constructed. We feel that the degree of success achieved lends further support to the network structure. We have investigated some simple microcrystallite models and our calculations will show that it would be necessary to add further refinements (such as large internal strains) to these in order to achieve the same degree of agreement with experiment.

In view of the uncertainties regarding the stucture of amorphous Si and Ge, it is fortunate that there exist well-defined metastable crystalline structures of Si and Ge which have large unit cells. These are the so-called BC-8 and ST-12 structures.[5] They have already served to test ideas regarding electronic properties[6–8] of the amorphous forms, and they may similarly serve to test our approach to the vibrational problem. A preliminary calculation of this type has been reported[9] and compared with Raman data for Si III (BC-8) and Ge III (ST-12). We will present here additional calculations for the BC-8 and ST-12 structures, as well as results for certain clathrate structures[10]

with even larger unit cells. Experimental data on Si-Na compounds in which the silicon atoms form these structures may soon be available.

Finally, we present predictions for inelastic neutron scattering in amorphous Si and Ge. In the limit of large momentum transfer, this provides a direct measurement of the vibrational density of states without the complication of any weighting due to matrix elements as in the Raman and infrared experiments. For smaller momentum transfer we find an oscillation of scattering intensity between low- and high-energy loss as the magnitude of the momentum transfer changes by about 1.5 $Å^{-1}$ (for Ge). This behavior is well explained in terms of the character of modes at the upper and lower ends of the spectrum, and it is rather different from that predicted for a polycrystal.

We shall begin with a short review of past and prevailing theoretical ideas and a summary of the available experimental data.

II. REVIEW OF THEORY AND EXPERIMENT

A. Theoretical background

Our intention here is not to give a full review of theoretical ideas in this area, but merely to set the scene for the results of the following sections by mentioning some relevant previous work. Recent reviews have been given by Bell,[11] Dean,[12] Lucovsky,[13] and Böttger.[14]

In many amorphous solids there is short-range order (usually meaning nearest-neighbor coordination only) similar to that of crystalline phases of the same composition. In such cases the vibrational spectrum is found to strongly resemble that of the crystal. The finding of Smith *et al.*[15] that this is true for amorphous Si and Ge (see Sec. II B) is thus typical of many amorphous solids. Most of these are much more complicated than Si or Ge, and it is difficult, in general, to pursue the matter further except to say that it is indicative of the short range of the dominant interatomic forces. The short range of such interactions would seem, however, to be a necessary rather than a sufficient condition for the invariance of major features of the spectrum, and the nature of the modes responsible for the various features must be studied to give an adequate explanation of their lack of dependence on structure. The classic analysis of this kind was that undertaken by Bell and Dean[11,12] for SiO_2. They performed extensive numerical calculations for random-network models and associated each of the various peaks on the vibrational spectrum with modes of a particular local character, in terms of the bending and stretching of bonds. Even SiO_2, however, is a comparatively complex system, and the picture evolved by Bell and Dean is necessarily less tidy than that given below for Si and Ge. The comparative simplicity of the latter and the well-developed theory of electronic and vibrational properties of their crystalline phases make them ideal prototypes for the theoretical study of amorphous solids in general.

The numerical calculations of Bell and Dean used special techniques[11] to find the eigenvalue spectrum, rather than direct diagonalization of the dynamical matrix. This enabled them to deal with rather large random-network clusters of several hundred atoms. However, the advantages of this procedure are somewhat diminished when one considers the problem of estimation of Raman and infrared intensities, and also of identifying and projecting out boundary-related effects. These require the calculation of eigenvectors which are not directly given by the most efficient methods for computing eigenvalues. Bell and Dean thus calculated only small samples of eigenvectors, and this was found not to be entirely satisfactory, since the intensities did not vary smoothly from one eigenvector to the next. It is for these reasons that we have chosen to simply diagonalize dynamical matrices, representing relatively smaller models than those of Bell and Dean, but with more sophisticated boundary conditions. Although the development of more efficient procedures to treat larger models along the lines suggested by Bell and Dean is, in the long run, desirable, we believe that at present more can be gained from studying smaller clusters with better boundary conditions.

In this regard it might be noted that prior to the work of Bell and Dean, most interpretations of observed spectra had been based on the study of isolated clusters such as SiO_4 (see, e.g., Gaskell[16]). This is a highly questionable approach in any system which cannot be divided into strongly bound molecules which interact weakly. Only very recently has there been an effort to incorporate into this point of view a proper allowance for the interactions of the molecular unit with its environment.[13,17]

The $\vec{k}=0$ selection rule restricts Raman and infrared spectra to a series of sharp lines for crystals, while for amorphous solids the absence of periodicity allows all vibrational eigenvectors to contribute to the spectrum; so the Raman and infrared spectra both extend over the entire vibrational spectrum. Of course, this statement does not imply that the weighting of different parts of this spectrum need be similar. In practice, it is often the case that the infrared and Raman spectra are only moderately distorted by this weighting. Shuker and Gammon[18] asserted that theoretical considerations would lead one to expect a roughly constant weighting within each of the bands of which the Raman spectrum is composed. However, subsequent developments have not given much support

to this idea. In particular; as mentioned in Sec. VI B, the lowest-frequency bands have a striking variation of intensity in both Raman and infrared spectra. (See also discussion by Whalley and Bertie.[19])

Hass[20] estimated infrared intensities for SiO_2 on the basis of a point-charge model, and Bell and Dean have made some preliminary calculations of the same sort, as well as calculations of Raman intensities for SiO_2 using a bond-polarizability model analogous to the one used here. We might note here that, while the choice of the appropriate zeroth-order approximation for infrared intensities is an obvious one in most cases, being given simply by a point-charge model, in the case of a homopolar solid such as Si or Ge this gives zero. Here it is necessary to invent a more elaborate model, which we undertake in Sec. III C.

The key to several of the interpretations of the experimental and numerical results which we shall give is the consideration of a simplified model in which all but the nearest-neighbor central forces are neglected and nearest neighbors are assumed to have *exact* tetrahedral symmetry. At first, this might seem an unreasonable model for a covalent semiconductor, since tetrahedrally bonded structures cannot even be stable with respect to such forces. Nevertheless, it does appear to be true that the central forces are the strongest forces at work in the determination of vibrational eigenstates. It has proved very useful, at every stage, to develop a clear picture based on these simplifications, which is then perturbed by the consideration of the effects of the smaller noncentral forces and distortions from local tetrahedral symmetry.

B. Experimental background

We know of at least five different experimental methods which have given information on part or all of the vibration density of states of amorphous silicon and germanium. These methods are Raman scattering,[15,21(a)–26] infrared absorption[27–29] or reflection,[30] low-energy electron tunneling,[31,32] high-energy electron energy loss,[33,34] and neutron scattering.[35] The most comprehensive data, as regards the variety of samples studied, have been obtained by Raman and infrared spectroscopy. We shall review the results of each of the above types of vibrational spectroscopy on amorphous Si and Ge as well as the results of studies on Si and Ge polymorphs.[9,36,37]

1. Raman scattering

Smith and his co-workers[15,21–23] were the first to obtain Raman spectra of amorphous Si and Ge as well as a number of related III-V amorphous semiconductors. A direct trace of a typical low-temperature (27-K) spectrum of amorphous Si is shown in Fig. 1. A first-order Stokes Raman spectrum is proportional to the factor $n(\omega, T)+1$, where $n(\omega, T)$ is the Bose-Einstein distribution at temperature T for vibrational energy ω. The anti-Stokes spectrum is proportional simply to $n(\omega, T)$, and so vanishes as the distribution function goes to zero. At 27 K and $\omega > 100$ cm^{-1}, $n(\omega, T) \ll 1$ (as can be seen by the absence of the anti-Stokes spectrum), and the Stokes spectrum is independent of the distribution function. The spectrum shown therefore differs from the vibrational density of states only by the factor $1/\omega$ dis-

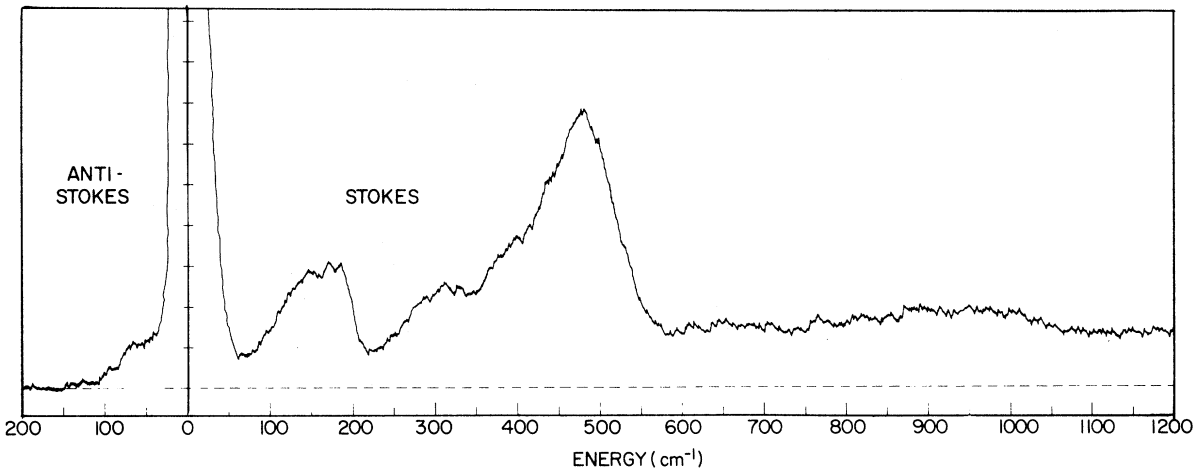

FIG. 1. Raman spectrum of amorphous Si at 27 K. The material was prepared by high-energy ion bombardment. Instrumental resolution is 10 cm^{-1}. The spectrum was excited by 0.24 W of 488-nm light and the measured peak height at 480 cm^{-1} is 35 photons/sec (Ref. 21).

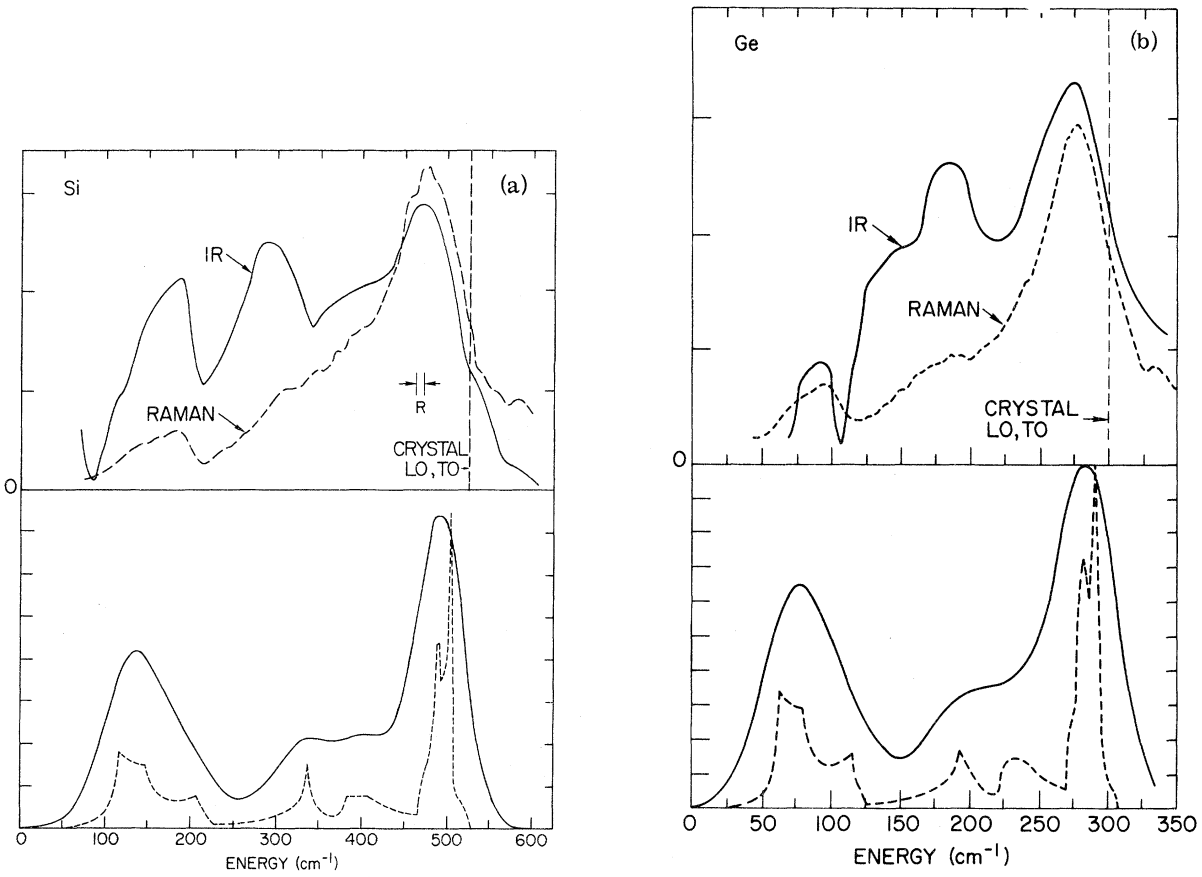

FIG. 2. (a) Top: Room-temperature infrared absorption constant (solid line) vs wave number for amorphous Si (Ref. 29). Also shown is the reduced Raman spectrum (dashed line) from room-temperature data (Ref. 21). Bottom: Density of states (dashed line) of crystalline Si from a fit to neutron-scattering data [Ref. 35(b)]. The solid line is the broadened density of states; the broadening is described in Ref. 21. (b) Top: Room-temperature infrared absorption constant (solid line) vs wave number for amorphous Ge (Ref. 29). Also shown is the reduced Raman spectrum (dashed line) from room-temperature data (Ref. 15). Bottom: Density of states (dashed line) of crystal Ge from a fit to neutron-scattering data [Ref. 35(b)]. The solid line is the broadened density of states (Ref. 21).

cussed in Ref. 18 and by factors accounting for the dispersion in the Raman coupling. Smith *et al.*[21] observed that for energies below about 550 cm^{-1} this Raman spectrum is similar to the vibrational density of states of crystalline Si, and they suggested that (i) the dispersion in the Raman coupling is a slowly varying function of frequency and (ii) the vibrational spectra of the amorphous and crystalline forms of Si are very similar. The broad continuum above the first-order spectrum ending at about 1050 cm^{-1} is probably second-order scattering; this is supported both by the temperature dependence[21] and the analysis given in this paper.

Smith *et al.* have also performed a variety of experiments to establish that the reported spectra are characteristic of amorphous Ge and Si and independent of method and temperature of preparation. Amorphous Si was prepared on substrates at temperatures from 300 to 750 K. Methods of preparation included vapor condensation of Si or Ge, chemical vapor deposition of Si from SiH_4, rf sputtering of Si and Ge, and high-energy ion bombardment of polished crystalline Si or Ge surfaces. No measurable differences in the Raman spectra were observed. Wihl *et al.*[24] have observed a difference in the location of the high-frequency peak of amorphous Ge prepared by the sputtering and electrolytic methods and relate this to a 1% difference in the material densities. To our knowledge no studies have been performed on samples prepared and maintained below room temperature.

The upper part of Fig. 2(a) shows the reduced Raman spectrum of amorphous Si. The reduction corresponds to multiplication of the Stokes spectrum by the factor $\omega/[n(\omega, T)+1]$. Shuker and Gammon[18] have pointed out that in the absence of matrix-element effects the shape of this reduced

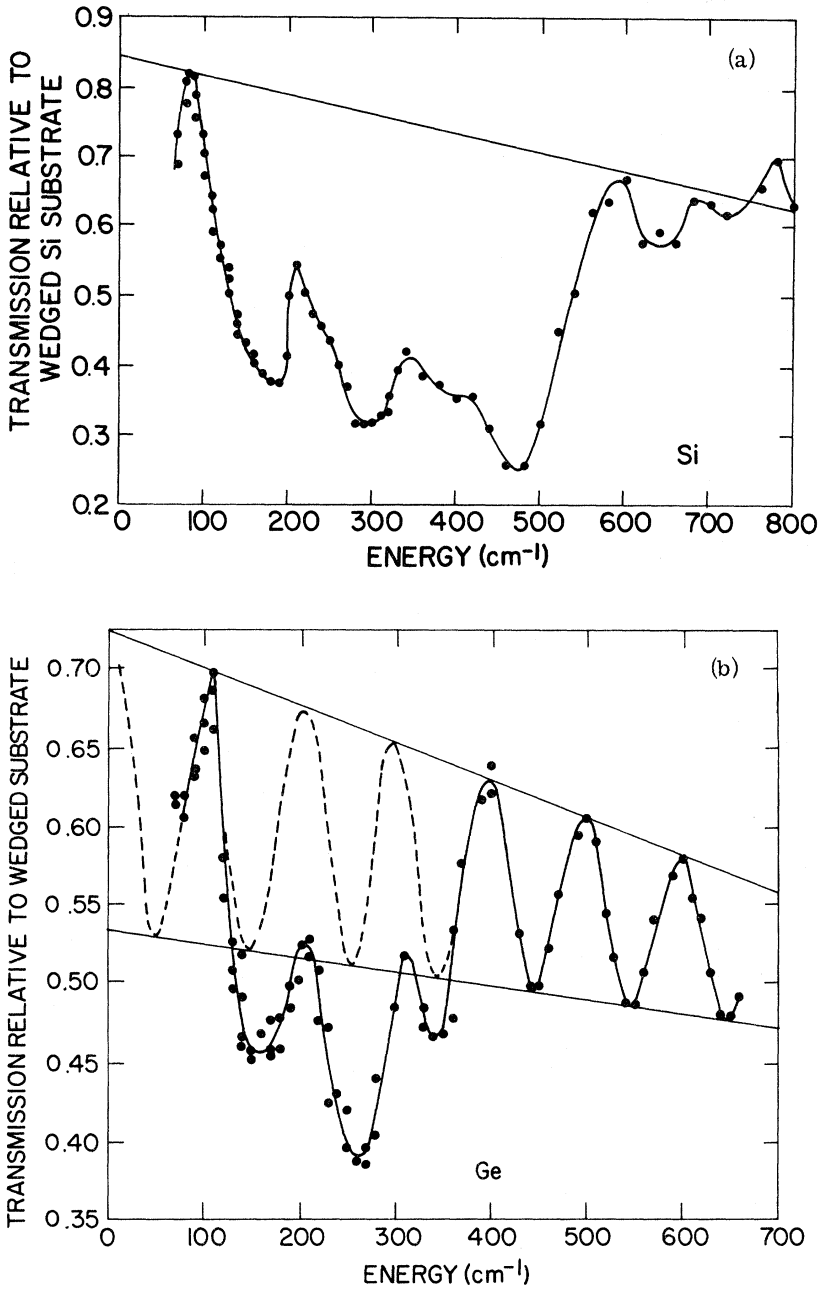

FIG. 3. (a) Transmittance of 37 μm of a-Si on both sides of a wedged high-resistivity crystalline Si substrate relative to a matched uncoated substrate. (b) Transmittance (solid line) of 25 μm of a-Ge on both sides of a wedged high-resistivity crystalline Si substrate relative to a matched uncoated substrate. The dashed curve is an estimate of the interference fringes in the transmittance (see Ref. 29).

spectrum would be that of the vibrational density of states. Figure 2(b) gives equivalent results for amorphous Ge.[15] The results of Wihl *et al.* [24] are in good agreement with those shown in Fig. 2. The lower parts of Figs. 2(a) and 2(b) show the crystalline densities of states, as well as broadened versions of them.[15,21] It is clear that the general features of the reduced Raman spectra are given by the crystalline density of states, appropriately broadened, although the higher-frequency modes of the reduced Raman spectra are relatively stronger.

2. *Infrared spectroscopy*

The infrared absorption spectra of Brodsky and Lurio[29] are also shown in Figs. 2(a) and 2(b). There is a well-defined peak in the middle of the spectrum where the Raman results show only a hint of structure; in addition, there are low- and high-energy peaks as in the Raman spectrum. However, because of the experimental difficulties in the far-infrared region, the relative strengths of the three peaks are not known precisely. We believe the Si data to be more reliable, the rea-

sons for which are easily seen from the raw data of Fig. 3. The complicating effects of multiple reflection interference effects and low absorption in the thin-film samples distort the Ge spectrum. The Si data are clearer mainly because of thicker samples, the higher frequency range, and a fortuitous masking out of the fringes because of thickness variations. In Fig. 4 we see that the absorption measurements of Prettl *et al.*[28] and the reflectance measurements of Stimets *et al.*[30] show relative intensities of the three peaks of amorphous Ge different from the results of Ref. 29. In the absorption spectrum (Fig. 4) of Prettl *et al.*[28] the two lower-frequency peaks are barely discernible as shoulders in the high-frequency peak. In contrast to this, the reflectivity data of Stimets *et al.*[30] have been analyzed to give an absorption spectrum (Fig. 4) with the three distinct peaks, but the two lower-frequency peaks are relatively more enhanced than in the Brodsky-Lurio results. For the sake of comparison with our calculations below, we shall use the amorphous Si data of Fig. 2. However, the lowest-frequency peak should be regarded with some caution, in light of recent microwave loss measurements[30(b)] which suggest that mechanisms other than lattice vibrations might be important for low frequencies.

The total strength of the infrared absorption in amorphous Ge and Si is substantial compared to the usual lattice absorption of the closely related crystalline III-V compounds. The integrated absorption strength, expressed as $\Delta\epsilon$, the contribution to the low-frequency dielectric constant, is about 0.5 for amorphous Si and 0.3 for amorphous Ge.[29] Typical values for crystalline III-V's are around $\Delta\epsilon = 2$. Although some workers[28,30] have attributed the disorder-induced absorption in amorphous III-V's to a redistribution of the crystalline oscillator strength, it is clear that in the case of Si and Ge, where there is no first-order oscillator strength for the crystal, the spectrum cannot be viewed as a broadening or redistribution of processes allowed in the crystal.

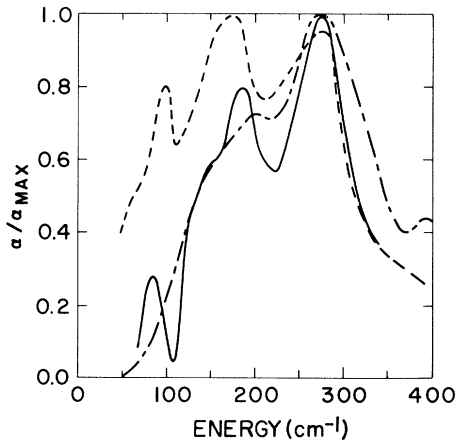

FIG. 4. Comparison of the absorption constant vs wave number for amorphous Ge as determined by three different groups. Solid line: Brodsky and Lurio, Ref. 29, $\alpha_{max} = 166$ cm^{-1}; short-dashed line: Stimets *et al.*, Ref. 30, $\alpha_{max} = 164$ cm^{-1}; dash-dotted line: Prettl *et al.*, Ref. 28, $\alpha_{max} = 910$ cm^{-1}.

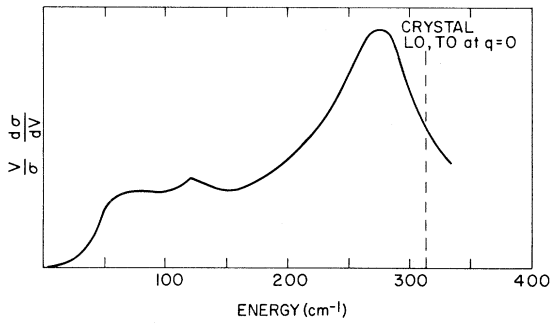

FIG. 5. Tunneling density of states of amorphous Ge as deduced by Ladan and Zylbersztejn (Ref. 31). Here σ is the tunneling conductivity at the voltage $V = \hbar\omega/e$.

3. *Tunneling spectroscopy*

Ladan and Zylberstejn[31,32] have deduced the vibrational spectrum of amorphous Ge from phonon-enhanced electron tunneling through a Ge barrier. Their samples were evaporated onto 77 K substrates, but apparently exposed to ambient temperatures before being cooled to 4.2 K for measurement. As seen in Fig. 5, their results are qualitatively similar to the reduced Raman spectrum. We have not made any calculations of tunneling spectra.

4. *Electron-energy-loss spectroscopy*

Schröder and Geiger[33] have reported that high-resolution (5-meV) detection of the energy loss of 25-keV electrons can show features of the two phonon spectra of amorphous Si and Ge. More recently Schröder[34] reported that the single-phonon density of states is also observable by similar techniques. We make no effort to interpret these results.

5. *Inelastic-neutron-scattering spectroscopy*

Axe *et al.*[35] have preliminary results for the elastic-neutron-scattering spectrum for the low-frequency branch of the amorphous Ge. The results show that the low-frequency peak in the density of states of amorphous Ge is slightly broader and shifted to lower frequency compared with the transverse accoustic (TA) peak of the crystalline form. As we show below, the neutron technique

should be a good measure of the entire vibrational density of states, particularly if proper account is taken of the dependence of the spectrum on momentum transfer. However, our treatment does not give any explanation for the observed small shift of the TA peak.

6. *Polymorphs and clathrates*

There exist several crystalline polymorphs of Si and Ge. These phases are generally obtainable by various high-pressure and -temperature cycles.[5] Several of the polymorphs are metastable at ambient conditions after the completion of the pressure-temperature processing. In addition, there are complicated cagelike forms of Si with small amounts of Na which have clathrate crystal structures.[10] Raman spectra of Ge III (ST-12), Si III (BC-8), and wurtzite Si (2*H*-4) have been reported[9,36,37] and analyzed with a model similar to that used below for the clathrates. We have tried to observe Raman scattering from Si clathrates and have yet to succeed.

III. INGREDIENTS OF A THEORY

A. Structure

Our numerical calculations are, in essence, simply normal-mode calculations for various models intended to represent amorphous Si and Ge. A prerequisite for the calculation is then a set of coordinates defining the positions of all the atoms in the model. It is desirable that the model contain many atoms in order adequately to represent a nonrepeating structure, but it is also desirable that the dynamical matrix, which is of the order of three times the number of atoms (n) be small enough to be conveniently diagonalized. The gains in resolution, volume-to-surface ratio, and limiting wavelength all vary as fractional powers of n, while the calculation cost tends to increase as n^5 for large n. These conditions limited the size of models to about 90 atoms, with relatively little to be gained from considerable increase in cost and/or computational complexity for larger numbers of atoms. Since simple clusters of 90 atoms tend to have about 60% of the atoms with at least one surface bond, boundary conditions are quite important. This is especially true in calculations of infrared intensities, as will be discussed in Sec. III C.

We have done calculations on three types of representation of the continuous random network. These are hand-built periodic "Henderson" models,[4] computer-generated periodic-defect models, and hand-built relaxed-cluster "Polk" models[38] with quasiperiodic boundary conditions. It might be noted that the computer-generated cluster models with relatively low distortions and no dangling bonds have only very recently become available.[39] It would be most desirable if low-distortion periodic models could be generated by computer, but this goal has yet to be achieved. (See, however, Ref. 40.)

The first type of model is constructed by filling a cube, which would contain 64 atoms in a diamond-cubic arrangement, with tetrahedral units connected in such a way that (i) a substantial number of fivefold rings of bonds are present, (ii) all atoms with bonds protruding through the surface can be connected with other atoms in the structure displaced by unit vectors parallel to the cube edges, and (iii) distortions from tetrahedral bonding at each site are as small as possible. These models can therefore be considered as repeating crystal structures with large unit cells. Henderson[4] has built such a model with 61 atoms and an rms angular distortion of 12.5°. We have built another such structure with 62 atoms with an distortion of 14.9°. These models have much greater angular distortion than the 7.1° of the Polk model because the severity of the constraint of periodic boundary conditions requires considerable relaxation of the requirement of small distortions from tetrahedral symmetry.

The second type of model is derived from a diamond-cubic structure by a computer procedure which creates defects containing fivefold rings of bonds. In this procedure an atom is selected at random and removed. Those atoms which had been neighbors of the removed atom are bonded to one another. This reduces the number of sixfold rings of bonds, creates fivefold rings, and also disorders the structure in some sense. At each stage in the process tests are made to ensure that no fourfold rings of bonds are created. When the desired number of defects have been created, the structure is relaxed in such a way as to minimize the Keating[41] elastic energy. Structures created in this way have relatively large distortions and are consequently of little direct use, but it is interesting to compare the results which arise from them with those of other models.

The third type of random-network model is derived from the tetrahedrally bonded cluster described by Polk.[2] These clusters have a good deal less distortion from tetrahedral bonding than do the periodic models. They present the problem of the treatment of surface effects. Bell and Dean[11,12] used "fixed" and "free" boundary conditions. The following quasiperiodic boundary conditions seems preferable. Each atom with a surface bond is bonded to another such atom displaced by a vector chosen to minimize the deviations from tetrahedral bonding. Pairs of bonds to be so connected are chosen so that fourfold rings of bonds do not occur. In this way we have created models with very low

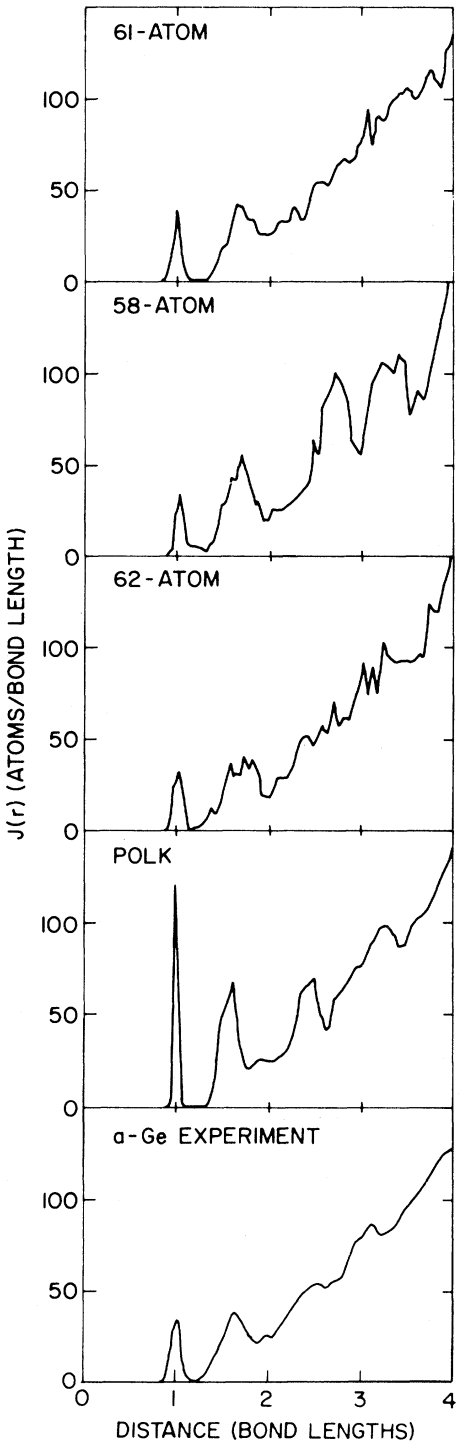

FIG. 6. Radial distribution functions for some of the model structures used in the calculations of vibrational spectra. "61-atom" is a periodic hand-built computer-refined structure due to Henderson; "62-atom" is a similar structure built as part of this work; "58-atom" is a periodic defect structure derived from diamond cubic; "Polk" refers to low-distortion nonperiodic models of the type studied by Polk. (See Table I for distortions and ring statistics of these models).

TABLE I. Summary of structural properties of models.

Model	$(\Delta^2 r)^{1/2}/\bar{r}$	$(\Delta^2\theta)^{1/2}$	fivefold rings/atom	sixfold rings/atom
61	3.8%	12.3°	0.41	0.90
62	4.3%	14.9°	0.42	0.85
58	3.5%	12.5°	0.38	1.07
Polk[a]	1%	7°	0.38	0.90

[a]Does not include distortions associated with quasiperiodic boundary bonds. Typical boundary-bond angular distortions are 15°–20°. Boundary-bond distance distortions are constrained to be zero.

interior distortion, and distortions at the surface only somewhat higher than for periodic models. For properties which are particularly sensitive to the distortion, which include infrared absorption, it is still desirable to count only contributions from the internal part of the cluster (see Sec. III C).

A comparison of some of the models for which vibrational properties were computed is given in Fig. 6, where we show radial distribution functions, and in Table I, where we indicate bond length and angle distortions and ring statistics for representatives of the three types of structure.

B. Force constants

The phonon dispersion relations of the crystalline group-IV semiconductors have been investigated with extraordinary thoroughness by means of neutron scattering,[42] both on and off the principal symmetry directions. Various semiempirical models have been used to interpolate and interpret the data. In all of these, nearest-neighbor central forces are the largest forces involved. If smaller short-range forces which resist angular distortions are also included, one obtains a qualitatively satisfactory spectrum. If one demands a very high degree of agreement with the experimental data, it may be necessary to include quite distant interactions, as Herman showed.[43] This should not, however, be allowed to obscure the essential simplicity of the phonon dispersion relations in these materials.

If simple forces resisting angular distortions are to be incorporated in a force-constant scheme there is some arbitrariness in the choice of the form of such forces. The prescription of Keating[41] is to use a term in the potential energy of the form

$$\frac{3}{16}\beta \sum_{l\{\Delta\Delta'\}} [(\vec{u}_l - \vec{u}_{l\Delta})\cdot\vec{r}_{\Delta'}(l) + (\vec{u}_l - \vec{u}_{l\Delta'})\cdot\vec{r}_{\Delta}(l)]^2 \quad (1)$$

to represent such bond-bending forces. In addition, there is the central-force term, which may be written

$$\frac{3}{4}\alpha \sum_{l\Delta} [(\vec{u}_l - \vec{u}_{l\Delta}) \cdot \hat{r}_\Delta(l)]^2, \qquad (2)$$

where the expression in square brackets is the compression $C_\Delta(l)$ of the bond Δ of atom l. Here (and throughout this paper) α and β are bond-stretching and bond-bending force constants, respectively; the sums are on atoms l and their nearest neighbors Δ; $\hat{r}_\Delta(l)$ is the unit vector from the equilibrium position of atom l to that of its neighbor $l\Delta$; $\vec{u}_l$ and $\vec{u}_{l\Delta}$ are the displacement vectors of these atoms. Equation (1) may be derived, in the harmonic approximation, from the assumption of a potential-energy term which depends only on the scaler product of nearest-neighbor vectors.[41,44] The alternative "valence-force" model[45] is derived from the replacement of this scalar product by the corresponding interbond angle. Yet another choice is that of the Born model,[46] in which the potential energy is

$$\frac{3\beta_{\text{Born}}}{4} \sum_{l\Delta} [(\vec{u}_l - \vec{u}_{l\Delta}) \cdot \hat{r}_\Delta(l)]^2 + \frac{\alpha_{\text{Born}} - \beta_{\text{Born}}}{4} \sum_{l\Delta} (\vec{u}_l - \vec{u}_{l\Delta})^2 \quad .$$

Somewhat confusingly, α and β are also conventionally used here, but their meanings are not the same as in the Keating model—hence our designation "Born."

A priori, there is not much to be said in favor of any of these except that the first two, being rotationally invariant, avoid certain possible pitfalls inherent in the Born model.[47] Martin[48] has argued in favor of the Keating prescription, on the grounds that the identity which it implies, relating the three elastic constants of the diamond-cubic structure, is close to being satisfied by the experimental data. The Keating model is also attractive in that it is slightly more economical for computation than the valence-force model. We have chosen this prescription for the calculations presented here but do not wish to belabor the distinctions between it and the others, which are of little significance at the level of detail with which we are concerned.

By the same token the details of the phonon dispersion relations, such as the flattening of the TA nodes near the zone boundary,[42] which have been much discussed in terms of more forces of longer range, such as are incorporated in the shell model[49] and the bond charge model,[50] as well as extensions of the above formulations, will not concern us here.

However, the existence of such forces must be borne in mind in the interpretation of our results. As well as influencing the shape of the spectrum and the character of the modes directly they may also be reflected in the structure itself. Most model structures have been refined by the minimization of the energy without regard to these more distant forces. It may be argued, for instance, that the small width of the second-nearest-neighbor peak in the RDF of the Polk model, relative to the experimental RDF, is due to the neglect of such forces.

C. Matrix elements

Having calculated the vibrational modes of a given structure with suitable force constants, it remains to assign infrared and Raman activities to these modes.

Both activities may be written as complicated integrals over the electronic states of the valence and conduction bands.[51,52] However, even in crystals where the calculation of such electronic states is relatively straightforward, such a first-principles calculation is a formidable undertaking. In In the case of diamond cubic Si and Ge, for which the $\vec{k} = 0$ TO modes are Raman active (and not infrared active), only Swanson and Maradudin[53] have attempted such a calculation to date.

The expressions which we will use to calculate Raman and infrared activities are based on a localized point of view, in which these quantities (or rather, the transition probabilities associated with them) are written as sums of local contributions. Short-range order and local symmetry can then be used to restrict the allowed forms to a few possibilities, which may be weighted with adjustable coefficients. Presumably the Wannier-function formalism is the key to the relation of such a picture to that which involves integrals of matrix elements of extended wave functions. While one may appeal to this in principle, it is difficult to follow through in practice, and we appeal rather to the general success of theories based on the local picture, as practiced by Phillips[50] and others in recent years, as a justification for such an approach. A resort to the band picture might be necessary if, for instance, any significant dependence of the Raman spectrum on the exciting frequency were to be found. To date, no such dependence has been reported. It should be noted, however, that the frequencies which have been used are rather close together.

The transition probability whose square determines infrared activity is proportional to the dipole moment $\vec{M}$ associated with the vibrational mode. If we write the displacement of atom l in a given vibrational mode as $\vec{u}_l$ then, to first order, the dipole moment is a linear function of $\vec{u}_l$. In keeping with our above remarks, we may try to approximate this function by a sum over all of the nearest-neighbor bonds of the system. However, if it is further assumed that each bond can be treat-

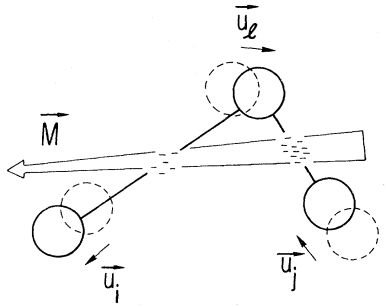

FIG. 7. Mechanism for infrared activity. During a vibration, bond charge moves from extended to compressed bonds, resulting in a local electric-dipole moment $\vec{M}$. The local moments cancel for modes of the diamond cubic structure, but they do not cancel in amorphous structures.

ed as having inversion symmetry about its center, as is reasonable for a homopolar material, and that a rigid translation of the bond can give no dipole moment, such a description will give identically zero for the induced dipole moment. To see this, consider the dipole moment associated with a given bond, which, by the second of the above conditions, may be written

$$\vec{M} = \overleftrightarrow{T} \cdot (\vec{u}_1 - \vec{u}_2). \tag{4}$$

Here $\vec{u}_1$ and $\vec{u}_2$ are the displacement vectors of the two atoms joined by the bond, in some given vibrational mode. Under inversion, the vector upon which $\overleftrightarrow{T}$ operates does not change sign, but $\vec{M}$ must do so, and this is incompatible with the invariance of $\overleftrightarrow{T}$, unless $\overleftrightarrow{T} \equiv 0$. This is the same argument as that applied by Lax and Burstein[52,54] to the diamond-cubic structure, but is here applied to a single bond. See also Zallen[55] and Chen and Zallen.[56]

Clearly it is necessary to consider contributions from more than one bond at a time, if a nonzero infrared activity is to be obtained. The obvious choice is take *pairs* of neighboring bonds. Denoting each atom by l and its nearest neighbors by $l\Delta$, we write

$$\vec{M} = \sum_{l\{\Delta\Delta'\}} [\vec{r}_{\Delta'}(l) - \vec{r}_\Delta(l)][(\vec{u}_l - \vec{u}_l) \circ \vec{r}_\Delta(l) - (\vec{u}_l - \vec{u}_{l\Delta'}) \cdot \vec{r}_{\Delta'}(l)]. \tag{5}$$

This formula may be interpreted as representing the dipole moment due to the transfer of charge from extended to compressed bonds (see Fig. 7). It may be reexpressed in various other forms. One of these, which is given in Appendix A, is especially convenient for the qualitative understanding of (5) and also for certain calculations. This is because if we attempt to use (5) for an isolated part of a fully bonded cluster, as is desirable in some cases where the surface termination is not fully satisfactory, we obtain large contributions from the surface, due chiefly to certain terms which identically cancel when summed over a fully bonded system. These terms are precisely the ones which are set aside when (5) is reexpressed as (A1).

We have not explored any further forms of the infrared activity, since (5) gives quite good results by itself.

The Raman activity of a mode is given by the induced polarizability. In this case, therefore, we are dealing with a second-order tensor which is a linear function of the displacements $\vec{u}_l$. Again we write this as a sum of contributions from individual bonds, imposing invariance with respect to translations and inversion. Even if we further restrict the range of possibilities by the imposition of cylindrical symmetry about the bond, so that each bond is to be treated precisely as a homopolar diatomic molecule, there remain three independent forms for the polarizability:

$$\overleftrightarrow{\alpha}_1 = \sum_{l\Delta} [\vec{r}_\Delta(l)\vec{r}_\Delta(l) - \tfrac{1}{3}\overleftrightarrow{I}]\vec{u}_l \cdot \vec{r}_\Delta(l), \tag{6}$$

$$\overleftrightarrow{\alpha}_2 = \sum_{l\Delta} \{\tfrac{1}{2}[\vec{r}_\Delta(l)\vec{u}_l + \vec{u}_l\vec{r}_\Delta(l)] - \tfrac{1}{3}\overleftrightarrow{I}\}\vec{u}_l \cdot \vec{r}_\Delta(l), \tag{7}$$

$$\overleftrightarrow{\alpha}_3 = \sum_{l\Delta} \overleftrightarrow{I}\ \vec{u}_l \cdot \vec{r}_\Delta(l), \tag{8}$$

where $\overleftrightarrow{I}$ is the unit dyadic. By collecting terms referring to pairs of neighbors, we may note that the first and third expressions depend only on the bond compressions $C_\Delta(l)$.

It is difficult to attribute relative degrees of importance to these expressions *a priori* since, as we noted in the Introduction, the first-principles expression for Raman activity is so complicated. However, there is one important distinction between the first expression and the other two. The latter vanish in the case of perfectly symmetric tetrahedral bonding, since in that case

$$\sum_\Delta \vec{r}_\Delta(l) = 0. \tag{9}$$

The first expression, on the other hand, has a quadratic dependence on the bond vectors $\vec{r}_\Delta(l)$ and hence does not vanish. If (9) were to be very small in a given structure, clearly the expressions (7) and (8) would be expected to contribute little to Raman activity. However, for random-network structures of interest, the quantity (9) typically has magnitude 0.2 times the nearest-neighbor distance, and $\overleftrightarrow{\alpha}_2$ and $\overleftrightarrow{\alpha}_3$ cannot be neglected on grounds of approximate symmetry.

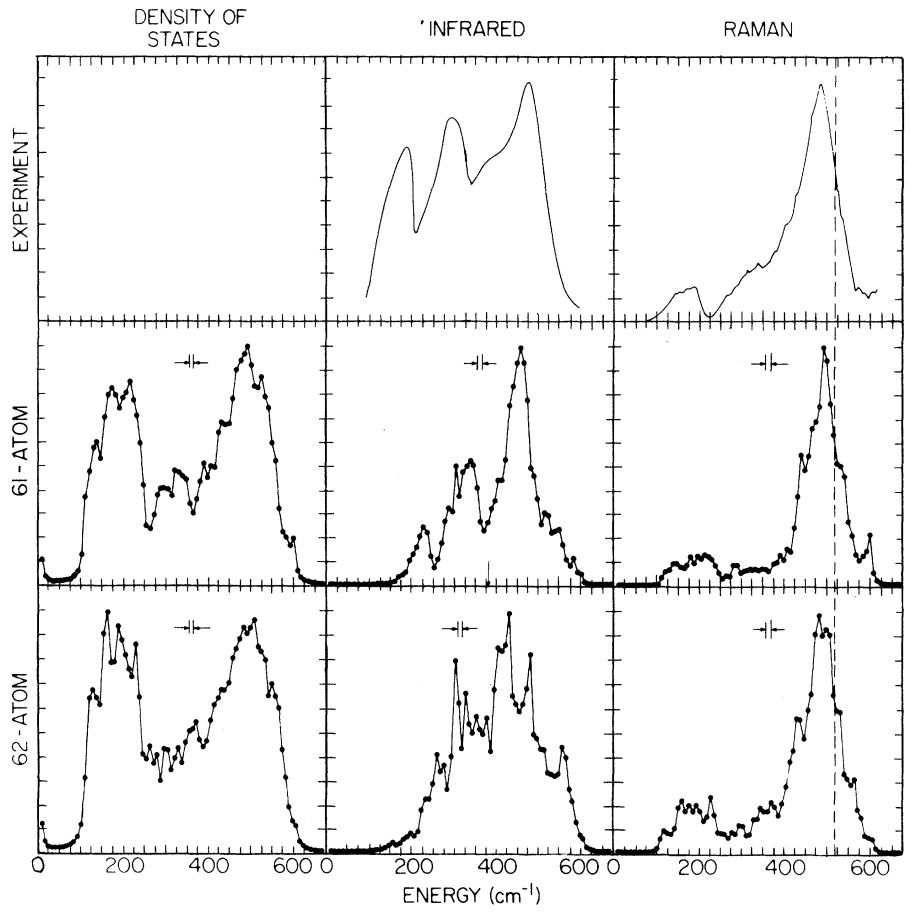

FIG. 8. Theoretical results for density of states, infrared absorption, and Raman scattering for 61- and 62-atom periodic models compared with the experimental data of Fig. 1 on amorphous silicon. The infrared absorption mechanism used in the theory is that of Eq. (5). The Raman mechanism is given in Eqs. (6)–(8) with the relative weights described in the text. The position of the maximum frequency mode for diamond cubic (the Raman-active TO mode) is indicated by the dashed line on the Raman graphs; the position of the density-of-states minimum near the center of the spectrum for diamond cubic with the force constants used in these calculations is indicated by the arrow at 380 cm^{-1} on the infrared-theory results. Spectra are formed by adding weighted Lorentzian contributions from $\vec{k}=0$ modes and are normalized to the same maximum value.

IV. NUMERICAL RESULTS

A. Results for hand-built periodic-random-network models

Figure 8 shows the results of a calculation using Henderson's periodic 61-atom random-network model and our 62-atom model and the theory of Sec. III compared with experimental data for Si. The force constants used are $\alpha = 0.475 \times 10^5$ dyn/cm, $\beta/\alpha = 0.2$. The choice of β/α is somewhat arbitrary, in view of the simplicity of this force-constant model. Values in the range 0.15–0.35 are consistent with various aspects of the phonon dispersion relations for the diamond-cubic structure. Keating's values, which were fitted to elastic constants, should not be assumed to have any universal validity.

The above value of β/α was chosen at an early stage in this investigation and was not varied thereafter. The position of the lowest peak in the spectrum depends on β in an essentially linear manner (as we shall show in Sec. VI A). It is clear that the theoretical peaks could be brought into slightly better agreement with the experimental ones by a small adjustment of β/α, but this would hardly add much to our understanding. Having fixed β/α, the value of α was fixed by fitting the zone-center TO frequency calculated for the diamond-cubic structure (indicated by a dashed vertical line in Fig. 8) to experiment. Another significant frequency, as will be discussed below, corresponds to the minimum in the LA-LO density of states for the cubic structure. This is indicated by the arrow in the result for the infrared spectrum of the 61-atom model.

The weighting of the various contributions to the Raman activity was determined as follows. The third mechanism is associated with a depolarization ratio of zero. The fact that the observed spectrum was found to have a similar shape in the HH and HV[21(b)] configurations[21(a)] with a depolarization ratio of 0.8 ± 0.1 then precludes any significant contribution from $\vec{\alpha}_3$, and it was accordingly given zero weighting. This leaves (apart from the over-all scale) only the ratio of the coefficients of $\vec{\alpha}_1$ and $\vec{\alpha}_2$ to be determined. By itself, $\vec{\alpha}_1$ provides a reasonable description of the upper half of the spectrum, but gives too little activity in the lower half. The inclusion of $\vec{\alpha}_2$ remedies this de-

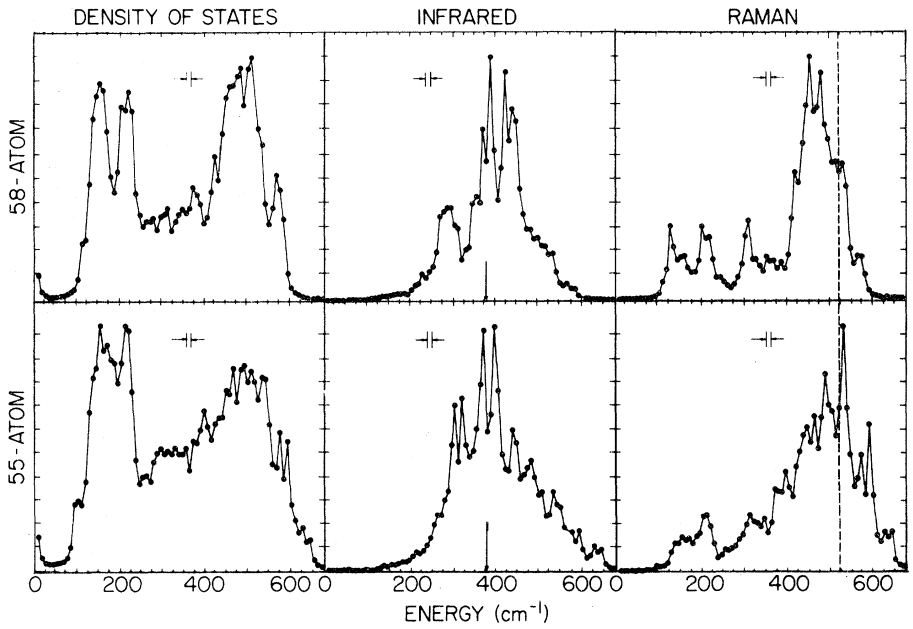

FIG. 9. Theoretical density-of-states, infrared, and Raman results for defect models. The maximum bond-length distortion for the 58-atom model is 10%. For the 55-atom model it is 30%. Infrared and Raman mechanisms are the same as for Fig. 8.

ficiency. The ratio 1:3 for the weighting of the two expressions was used in the calculations of Fig. 8.

In Sec. VI we shall give an interpretation of these and other results, i.e., an explanation of how these results arise from the assumed forms for force constants and activities. They play a primary role in our interpretation of the experimental data.

B. Other random networks

In Fig. 9 we show results for density-of-states, infrared, and Raman spectra for defect models. These spectra show certain sharp structures (e.g., the splitting of the lowest-frequency peak) which are associated with $\vec{k}=0$ modes of 64-atom diamond-cubic cell from which the models were derived. Nonetheless, it appears that there is a third peak in the center of the spectrum and a corresponding enhancement of the ir scattering from this peak, as for the hand-built model.

In Fig. 10 we show results for quasiperiodic models. There is a difficulty in obtaining meaningful ir spectra for such models, since a few strongly scattering regions with large distortions can dominate the spectrum. (The ir contribution

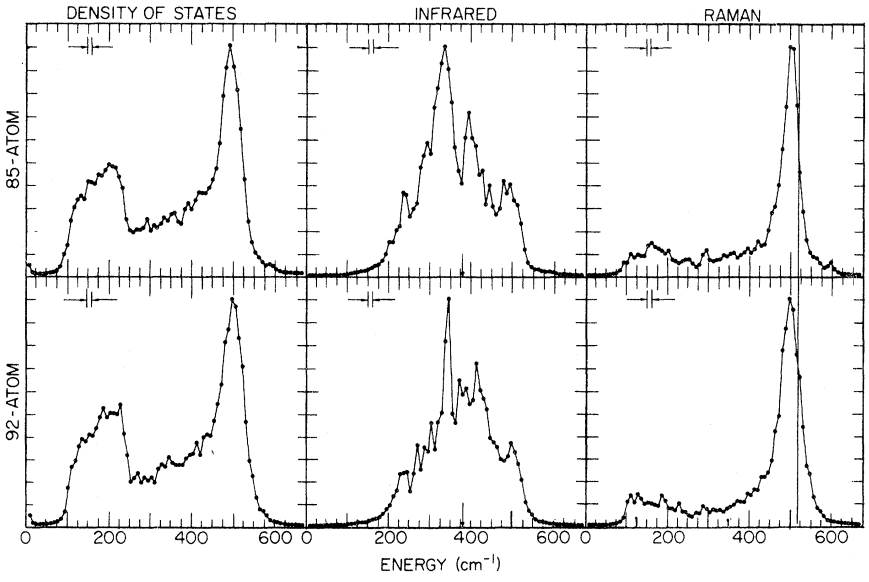

FIG. 10. Theoretical density-of-states, infrared, and Raman results for 85- and 92-atom quasiperiodic Polk models. These models have very low interior distortions, but large effective angular distortions at the boundaries. The Raman mechanism for these calculations was taken as a sum of the mechanisms of Eqs. (6)–(8) with equal coefficients. Only the *HH* spectrum is shown. The infrared mechanism is the same as for Fig. 8. Spectra are formed from contributions of the normal modes of the finite clusters.

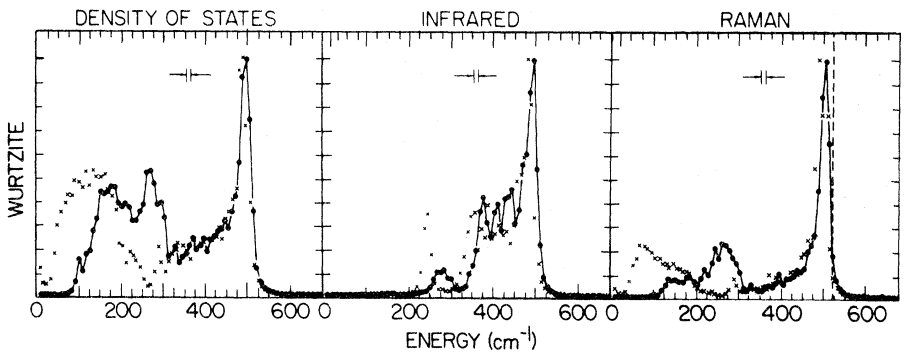

FIG. 11. Theoretical density-of-states, infrared, and Raman results for a microcrystallite model consisting of a strain-free spherical cluster of the wurtzite structure containing 64 atoms. Calculations for fixed (connected points) and free (×'s) boundary conditions are shown. The Raman mechanism is the same as for Fig. 8.

from a given atom is proportional to its deviation from tetrahedral symmetry. See Appendix A.) We attempted to minimize these effects by weighting the contributions of modes to the spectra (and the density of states) by their projection on the 36 fully bonded interior atoms in the cluster, i.e., by the sum of the squares of the components $\vec{u}_e$ associated with these atoms. This reduces the effects of boundary-condition-induced modes. However, this was judged still to be unsatisfactory, and calculations were therefore performed in which only the interior bonds contributed to the infrared matrix element. This is done by using the alternative form (A1) and summing only over interior atoms. [Use of the original form (5) would lead to difficulties in this case.]

Of significance is the relative sharpness of the uppermost peak of the density-of-states and Raman spectra compared with the periodic models. This appears to be associated with the lower angular distortion for the interior bonds of this model. The experimental results, interestingly enough, seem to be in better agreement with the more distorted models.

C. Microcrystals

Microcrystallite models have been proposed to explain certain aspects of electron diffraction on amorphous Ge. A microcrystal presumably is a region of well-ordered material separated by an identifiable boundary from other well-ordered regions. (By contrast, the random network would be regarded as structurally homogeneous.) Because of the boundaries, a small microcrystallite would not rigorously obey the usual k selection rule in Raman scattering or infrared absorption. To investigate this we examined spectra from approximately spherical 64-atom samples of diamond or wurtzite-structure models. These models represent quite small microcrystals and have many surface bonds. Even so, the Raman scattering seems to indicate a very sharp crystallike TO peak (see Fig. 11). To broaden this peak, it appears that internal strains comparable with those in the random-network model would be necessary.

Note that, according to the arguments of Appendix A, the infrared activity calculated here for a microcrystal arises entirely from surface contributions.

D. Polymorphs

In Tables II–V we give the mode identification and intensities for the infrared and the three Raman mechanisms of Eqs. (6)–(8) for the BC-8, ST-12, 136-atom, and 46-atom clathrate structures. (The numbers refer to the number of atoms per cubic cell.) The Raman mechanisms are given

TABLE II. Calculated spectra for the 136-atom clathrate (silicon). Lines with relatively large intensity are underlined.

Energy (cm^{-1})	Type	Relative Intensities: Infrared	A	B	C
137	F_{2g}		0.000	0.006	
142	E_g		0.000	0.020	
194	F_{1u}	0.003			
232	F_{1u}	0.003			
236	F_{2g}		0.000	0.000	
278	F_{1u}	<u>8.907</u>			
279	F_{2g}		0.000	0.018	
321	A_{1g}				<u>0.182</u>
390	E_g		0.002	0.000	
401	F_{1u}	<u>0.315</u>			
418	A_{1g}				0.032
435	F_{2g}		0.036	0.000	
452	F_{1u}	<u>0.615</u>			
491	F_{1u}	0.012			
492	F_{2g}		<u>1.149</u>	0.000	
499	A_{1g}				0.015
504	E_g		0.006	0.000	
505	E_g		<u>1.442</u>	0.002	
507	F_{1u}	<u>0.051</u>			
510	F_{2g}		1.116	0.003	
510	F_{2g}		0.000	0.000	
517	E_g		0.176	0.000	

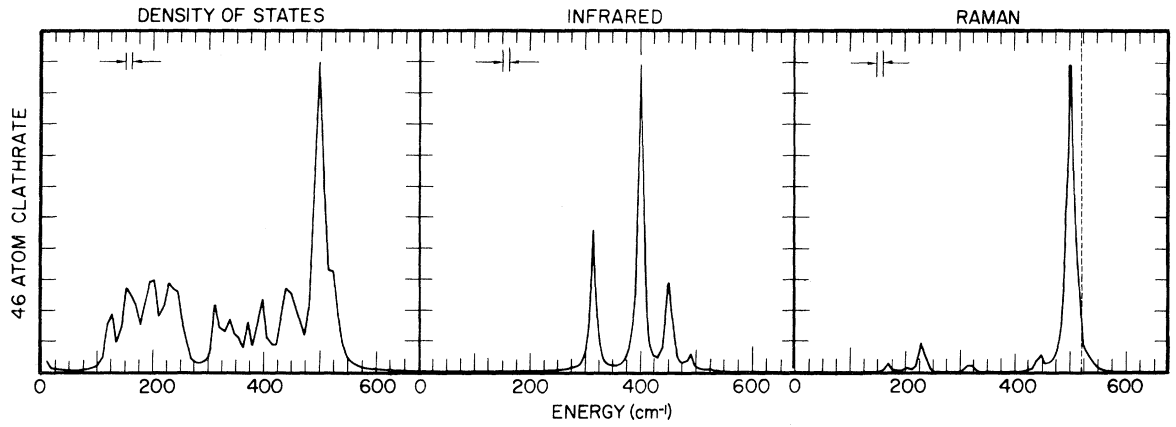

FIG. 12. Theoretical density-of-states (of 138 $\vec{k}=0$ modes), infrared, and Raman spectra for a clathrate structure with 46 silicon atoms in the unit cell. Mechanisms are the same as for Fig. 8.

separately, since it is not at all clear that the weighting of various terms used in Sec. V A should apply to these structures.[10] Both infrared and Raman intensities are divided by the number of atoms in the unit cell and multiplied by a constant which is the same for all structures. It might be noted that in these structures there is a distinct tendency for the Raman intensities to be highest for the highest-frequency modes, while the ir intensity is highest in center of spectrum. This behavior is similar to that found for random-network results, we give in Fig. 12 a spectrum of Raman and infrared intensity as well as density of $\vec{k}=0$ modes for the 46-atom clathrate.

TABLE III. Calculated spectra for 46-atom clathrate (silicon). Lines with relatively large intensity are underlined.

Energy (cm^{-1})	Type	Relative intensities: Infrared	A	B	C
120	F_{2g}	0.001	0.000	0.000	
153	F_{1u}				
168	E_g		0.000	0.008	
201	F_{2g}		0.000	0.003	
206	F_{1u}	0.042			
226	E_g		0.004	0.002	
231	F_{2g}		0.003	0.030	
240	F_{1u}	0.002			
312	F_{1u}	6.627			
317	F_{2g}		0.000	0.012	
332	F_g		0.002	0.000	
355	A_{1g}				0.411
398	F_{1u}	14.114			
435	F_{2g}		0.018	0.003	
444	E_g		0.020	0.010	
450	F_{1u}	4.971			
455	A_{1g}				0.020
488	F_{1u}	0.801			
493	F_{2g}		0.432	0.003	
496	E_g		0.576	0.018	
497	F_{2g}		0.546	0.006	
502	F_{2g}		1.587	0.003	
506	F_{1u}	0.015			
509	A_{1g}				0.024
513	E_g		0.574	0.002	
523	F_{1u}	0.105			
536	E_g		0.124	0.002	

E. Other force constants

We have also done calculations on random-network models with Born-model force constants. Results for the Henderson 61-atom model are shown in Fig. 13, where it may be seen that there is no really significant difference from the Keating force-constant results, except for expected slight shifts in the relative positions of the various peaks.

V. INTERPRETATION OF EXPERIMENTAL AND NUMERICAL RESULTS

A. Density of states

We shall begin an interpretation of the experimental and theoretical results of the previous sec-

TABLE IV. Calculated spectra for Si III (BC-8). Lines with relatively large intensity are underlined.

Energy (cm^{-1})	Type	Relative intensities: Infrared	A	B	C
200	F_{2g}		0.000	0.063	
228	F_{1u}	0.039			
439	F_{2g}		0.003	0.147	
440	F_{1u}	110.274			
454	A_{1g}				2.327
480	F_{2g}		3.621	0.100	
529	E_g		1.18	0.206	

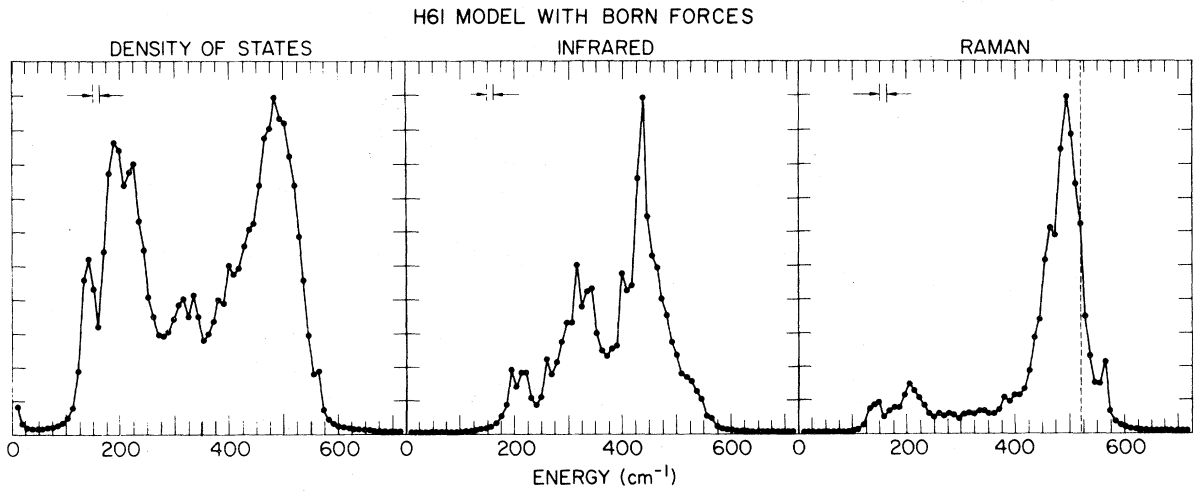

FIG. 13. Theoretical results for density-of-states, infrared, and Raman spectra for the 61-atom model with Born (rather than Keating) force constants. Here we have taken $\beta/\alpha_{\text{Born}} = 0.6$.

tions with an examination of the relationship between structure and the vibrational density of states $N(\omega)$, and give an explanation of the similarity of $N(\omega)$ for the amorphous and crystalline phases, discussing not just the two prominent peaks, but also some more subtle structure in the center of the spectrum.

TABLE V. Calculated spectra for Ge III (ST-12). Lines with relatively large intensity are underlined.

		Relative intensities			
Energy (cm^{-1})	Type	Infrared	A	B	C
70	B_1		0.001	0.001	
97	E	0.000	0.010	0.214	
101	A_2	3.765			
104	A_1		0.002	0.064	1.026
108	B_2		0.000	0.000	
115	E	0.007	0.000	0.068	
122	A_1		0.000	0.143	1.319
129	B_1		0.000	0.000	
167	A_2	79.674			
184	E	0.638	0.006	0.000	
204	E	0.249	0.046	0.016	
209	B_2		0.001	0.001	
218	A_1		0.007	0.030	0.354
245	B_1		0.009	0.000	
250	B_1		0.915	0.000	
252	A_2	0.477			
255	E	0.050	0.094	0.001	
259	B_2		0.089	0.000	
274	E	0.004	1.333	0.012	
293	E	0.030	0.030	0.046	
299	A_2	6.822			
303	E	0.065	0.090	0.004	
304	A_1		0.508	0.007	0.052
315	B_1		0.006	0.000	
316	B_2		0.000	0.000	

Figure 14 shows a histogram of the vibrational density of states for diamond-cubic Si derived from the Keating model with the same α and β parameters used for previously discussed structures. This simple model is known to be slightly inaccurate in the region of the TA peak,[42] but this level of detail hardly concerns us here.

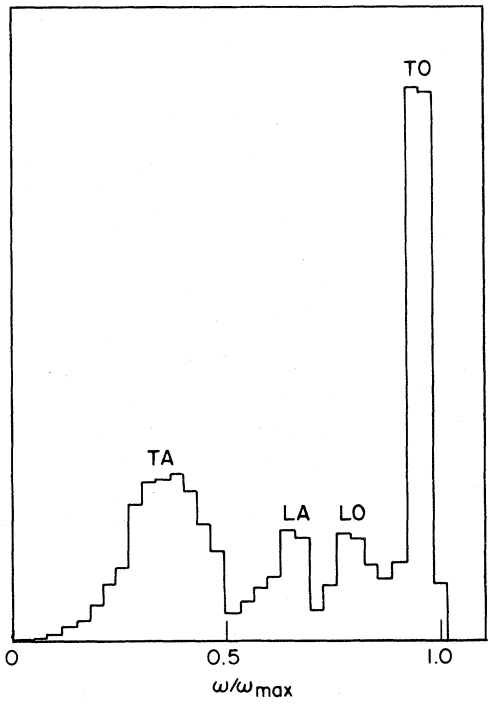

FIG. 14. Density of states for the Keating model with $\beta/\alpha = 0.2$ for the diamond cubic structure. Histogram is formed from frequencies for 4000 randomly chosen k points.

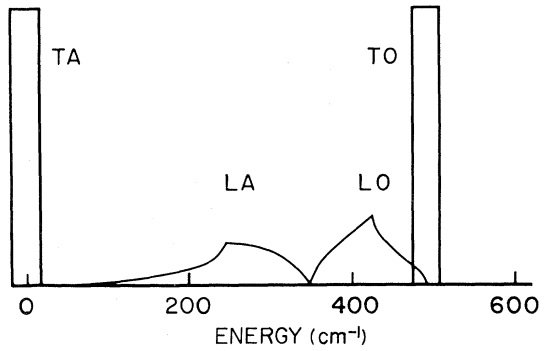

FIG. 15. Density of states for the Keating model with $\beta/\alpha = 0$ for the diamond cubic structure. δ functions at $\omega^2 = 0$ and 8α are represented by finite blocks.

The most prominent features of the density of states are the peaks at low and high frequency, arising from bands which are conventionally labeled TA and TO, respectively. The terms "transverse," "longitudinal," "acoustic," and "optical," as usually defined, are only meaningful in a periodic system. It is therefore inappropriate to use them in an amorphous system. One must instead concentrate on the bond-bending or stretching character of the modes, as Bell and Dean have emphasized,[11,12] if one wishes to develop a classification of modes which may have relevance to the amorphous case. One way of seeing the essential character of the modes is to take the limit in which the forces resisting bond bending (i.e., changes in interbond angles) go to zero, $\beta/\alpha \to 0$ in the notation of Sec. IV. The appropriate values of β/α for a description of the observed density of states are sufficiently small that this limit does not take us very far from reality. Figure 15 shows the nature of the density of states of the diamond-cubic structure in this limit. (We shall shortly explain the manner in which this was obtained, preferring for the moment to emphasize qualitative features while postponing related mathematics.) The TA and TO bands are completely flat and hence give δ functions in $N(\omega)$. The TA modes are now at $\omega = 0$. The existence of N zero-frequency modes, where N is the number of atoms, is easily demonstrated since the system has $3N$ degrees of freedom, and the requirement of constant bond lengths (and thus no change of elastic energy, if $\beta/\alpha = 0$) constitutes $2N$ linear constraints; so there are $3N - 2N$ such modes. These are pure bending modes. The origin of the second δ function is more obscure, since it is necessary to invoke tetrahedral symmetry to demonstrate its existence, as we shall shortly describe. However, examples of both kinds of modes can easily be set up on a closed ring of bonds, as shown in Fig. 16.

Note that the simple arguments given above regarding the existence of zero-frequency modes and the explicit construction given in Fig. 16, do not depend on the details of the diamond-cubic structure. All that is necessary for the existence of the first δ function is fourfold coordination, while for the second one tetrahedral symmetry is also necessary. The lack of dependence of these features on the topology of the structure is expressed in the following theorem, which also bears on the form of the rest of the density of states.

Theorem. The density of states for the case of equal central forces ($\beta/\alpha = 0$ in the case of Keating model), expressed as a function of $m\omega^2$, has the following form for a homopolar solid with perfectly symmetrical tetrahedral bonds. There is a δ function containing one state per atom at zero, another at 8α, and a band bounded by these values. Furthermore, this band is given by the spectrum of the simple Hamiltonian

$$H = \alpha \left(4I - \sum_{l\Delta} |l\rangle \langle l\Delta|\right), \tag{10}$$

which operates on (scalar) basis functions $|l\rangle$, one of which is associated with each site.[57]

A proof of this theorem has been outlined by Weaire and Alben.[58] A more economical version was given by Alben *et al.*,[59] the details of which are contained in Appendix B. The essential step

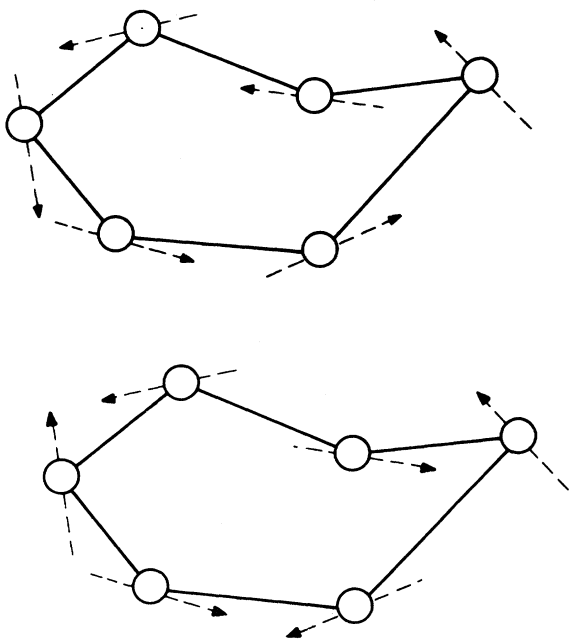

FIG. 16. Examples of localized modes, at frequencies $\omega^2 = 0$ and 8α, which may be formed on any closed ring of bonds if there is perfect local tetrahedral symmetry and central nearest-neighbor forces. The displacement vectors are in the plane of the bonds which belong to the ring and perpendicular to their bisector.

TABLE VI. Corresponding approximations for the electronic and vibrational problems.

Electronic density of states	Vibrational density of states
Realistic Hamiltonian (difficult)	Realistic Hamiltonian (difficult)
⇓	⇓
Simple tight-binding Hamiltonians	Simple force-constant Hamiltonians
⇓	⇓
Allow only short-range interactions	Allow only short-range forces; in fact, only central nearest-neighbor force constant α
⇓	⇓
Keep iteration parameters V_1 and V_2 fixed at the same values everywhere	Keep α fixed and treat all bond angles as $\cos^{-1}(\frac{1}{3})$
⇘	⇙
Equivalent problem: simple Hamiltonian one basis function per site (plus additional δ functions in the density of states)	

is the projection of the displacement vector $\vec{u}_l$ along each bond $l\Delta$. The projections thus defined form a new basis set of four (scalar) functions per atom. The analogy with tight-binding theory is at once apparent (four sp^3 orbitals per atom in this case). However, the four projections of $\vec{u}_l$ along the bonds $l\Delta$ are not independent. For the case of tetrahedral symmetry, the required constraint is simply that these projections add to zero. Translating this into tight-binding language, we have the condition for purely *p-like* wave functions. Thus by forcing wave functions to be *p-like* (which is accomplished by making the weighting of an appropriate part of the tight-binding Hamiltonian go to infinity and discarding the *s*-like part of the spectrum) we can make a precise analogy with the formulation of simple tight-binding theory by Thorpe and Weaire.[60] The above theorem then follows from the "one-band–two-band" theorem of the latter authors, which relates the band structure for simple tight-binding Hamiltonians to that of (11) together with various δ functions. The two δ functions correspond, respectively, to *p*-antibonding and *p*-bonding functions.

It is amusing that these two formalisms should, when peeled down to bare essentials, reduce to the study of the same Hamiltonian. The steps involved are indicated in outline in Table VI.

The above theorem is exact only for perfectly symmetrical tetrahedral bonding, such as in the case of diamond cubic (and was indeed used to produce Fig. 15 from the one-band spectrum[60]). However, we may expect it to apply in an approximate sense to structures which are only close to this condition, such as the random network. Remember that the $\omega = 0$ δ function would still exist in this case, according to the argument given earlier in this section, but the other one would be broadened by departures from exact tetrahedral symmetry. In addition, of course, both peaks have a finite width for finite β.

The picture evolved thus far is as follows. Any perfectly tetrahedral structure should have sharp peaks at low and high frequencies in the same places as the diamond-cubic structure, but if the tetrahedral bonding is not perfectly symmetric the upper one will have an additional broadening. The rest of the spectrum (which we shall discuss below) is contained in the region between the two peaks.

These conclusions are in good agreement with the results of Sec. V. In particular, we notice that the upper peak does broaden as distortions are increased in the structural models used for calculations.

A further calculation which may aid in understanding the above remarks is shown in Fig. 17. This shows that as $\beta \to 0$ the lower peak becomes sharper, being roughly proportional to β in width, while the upper one remains much the same, since most of its width arises from distortions (see also Fig. 2 of Ref. 58). The energy of the lower peak also tends towards zero as $\beta \to 0$. Incidentally, the asymmetry of the effects of distortion on the two peaks is somewhat disguised by the linear scale for ω which is traditionally used in these plots. The natural scale for a theoretical analysis is one proportional to the frequency *squared* (because this is the eigenvalue of the secular equation). Plotted on such a scale, the density of states for the diamond-cubic structure becomes exactly symmetric about its center for any force-constant scheme, such as that of the Born model, which involves only nearest-neighbor forces.

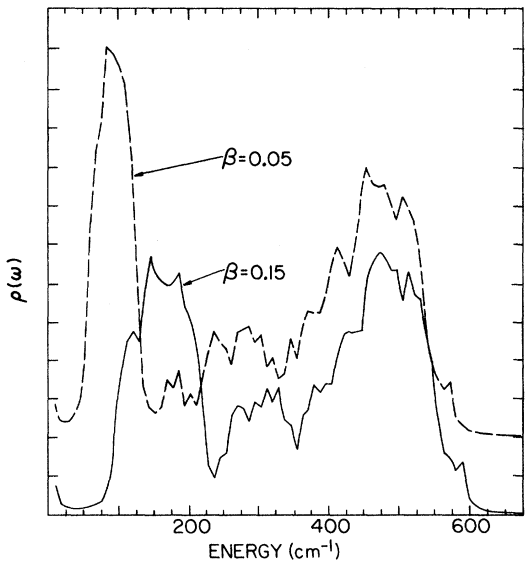

FIG. 17. Density of states $N(\omega)$ for the 61-atom periodic model for $\beta/\alpha = 0.15$ and 0.05, illustrating the change in the spectrum as $\beta \to 0$.

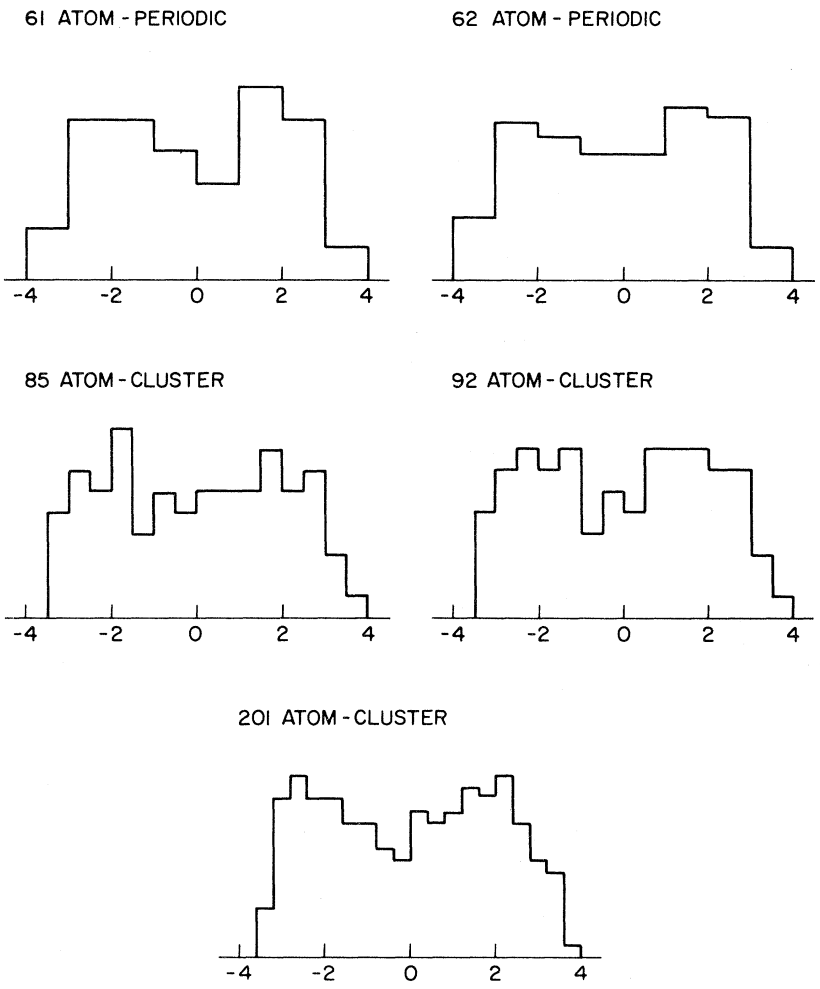

FIG. 18. One-band density of states for 61, 62, 85, 92, and 201-atom models. Histograms give the distribution of eigenvalues for $\vec{k}=0$ modes for 61- and 62-atom periodic models and for the finite number of modes of the 85-, 92-, and 201-atom cluster models. The 201-atom cluster result is probably representative of the (unbounded) Polk continuous-random-network model.

The central part of the density of states is *not* independent of topology, the particular form shown in Fig. 15 being for the diamond-cubic and related[61] structures only. According to the theorem discussed above and the work of Thorpe and Weaire,[60] this part of the density of states is closely related [through the one-band Hamiltonian (10)] to the lower half of the valence band of *electronic* states. The structure dependence of the latter has been of some interest. Thorpe and Weaire[62] predicted that the two-peaked structure found in the lower half of the valence band of the diamond-cubic phase of Si or Ge would be replaced by a single broad peak or plateau in the amorphous phase. This was subsequently confirmed by x-ray emission,[63] by x-ray photoemission spectroscopy (XPS),[64] and by uv photoemission,[65] but the force of the original argument was somewhat diminished by numerical calculations of the density of states[66] of the one-band Hamiltonian. These showed that the topological disorder of the Polk model is not, after all, quite sufficient to give a featureless spectrum, but rather one with a reduced, but still quite pronounced, dip in the center (see Fig. 18 for one-band results for various random-network structures). The explanation of the experimental results is therefore not conclusive, as was originally thought. It is interesting to ask if significant structure can be discerned in the corresponding part of the *vibrational* density of states. Does either theory or experiment for the amorphous phase contain the dip found between LA and LO peaks in the density of states of the crystal? The answer in both cases appears to be *yes*. This cannot be stated unequivocally on the basis of the experimental data alone since, if we examine the infrared data, it is not possible to say whether the dip which precedes the highest-frequency peak corresponds to the LA-LO splitting, which is what we have in mind, or the LO-TO splitting. However, if we examine the numerical results of Sec. V, which agree rather well with the experimental data, we can decide this, since the dip occurs almost exactly at LA-LO dip frequency of the corresponding crystal spectrum. Also, al-

most exactly half of the modes lie below the dip in which we are interested. This test strongly supports the former of the two possibilities considered above. Thus the three peaks in the density of states indicated by the observed ir and Raman spectra are considered to correspond, respectively, to modes of local character similar to the TA, LA, and LO + TO bands for diamond cubic, the LO and TO having merged because of the effects of distortions (see above). This unfortunately piles paradox upon paradox, since it is a result opposite to that which is found in the corresponding electronic measurements discussed above. A potential explanation, however, may be provided by matrix-element effects. As we shall see, these amplify considerably the effect of the middle peak in the ir spectrum. It is possible that other effects suppress the already diminished (compared to the crystal) structure expected on the basis of the one-band results for the electronic problem.

B. Matrix-element effects

All of the immediately preceding analysis is related to the vibrational density of states. We shall now consider how this is modulated by matrix-element effects to give the Raman and infrared spectra. We cannot claim to give any final explanations here because of the semiempirical approach used in the calculations, but nevertheless it would appear that much can be learned from them.

Again it is fruitful to consider the limit of purely central forces. In this limit the mean-square compression of bonds divided by the mean-square displacement varies as ω^2 over the entire spectrum. (See Appendix A.) Now the dominant contribution to the Raman tensor $\overleftrightarrow{\alpha}_1$ involves only the compression of each bond. If we neglect the correlations of compressions on different bonds, we are led to expect an ω^2 dependence of the Raman activity. (The other contribution $\overleftrightarrow{\alpha}_2$, which contributes mainly at low frequency, cannot be so written.) We can thus attribute most of the over-all increase of Raman activity with ω, apart from the low-frequency region, to the approximate ω^2 dependence associated with the mean-square compression of bonds.[67]

For the infrared spectrum a precisely similar argument can be used to relate the activity to the mean-square bond compression and hence to ω^2, but clearly this is not in keeping with the results of Fig. 18. The uppermost peak has a much lower activity than one would expect on such grounds alone. Indeed, here lies the principal qualitative difference between the infrared and Raman spectra. In Appendix A we give a proof of a theorem which explains the diminished contribution of this peak. It is shown that in the limit of purely central forces the matrix element (5) is of second order in the distortion from exact tetrahedral symmetry for the modes which contribute to this peak, while it is of first order for the spectrum as a whole. This tendency for the infrared activity to be greatest for modes near the center of the spectrum is seen in Fig. 19, where we have plotted the dispersion of the infrared activity per mode.

It is sometimes said that the differences between the two spectra can be simply understood by appeal to the results for the diamond-cubic structure, for which the TO $\vec{k} = 0$ modes are Raman active and not infrared active. This is far from obvious, since the latter statements follow simply from crystal symmetry without regard to the forces or matrix elements involved. The interpretation of the data for amorphous Si and Ge clearly requires consideration of both forces and matrix elements in some detail. If, for instance, $\overleftrightarrow{\alpha}_2$ and $\overleftrightarrow{\alpha}_3$ were the dominant forms of Raman matrix elements, the calculated Raman spectrum for the random network would be greatly changed, but the spectrum for the crystal would necessarily still consist of the single TO line.

VI. PREDICTIONS FOR NEUTRON SCATTERING

Inelastic neutron scattering at high-momentum-transfer vector $\vec{Q}$ has been advocated as a means of directly studying the phonon density of states of polycrystalline and amorphous elemental solids.[68] In the case of polycrystalline systems, this is justified by an argument to the effect that the experi-

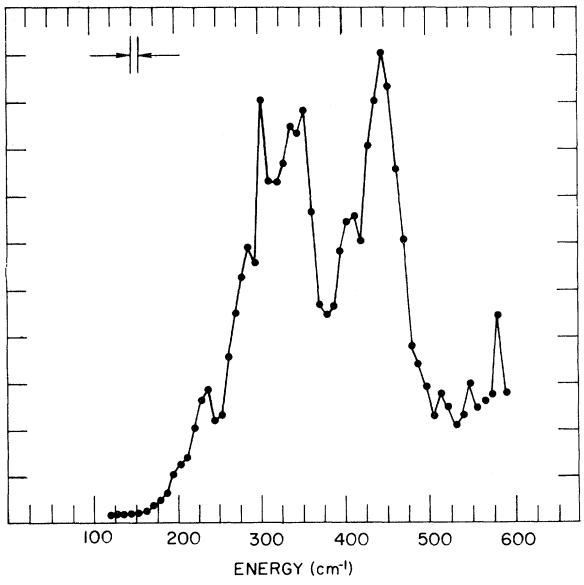

FIG. 19. Frequency dependence of the average intensity per mode for infrared absorption (61-atom model), as determined by dividing infrared absorption by density of states (see Fig. 8).

ment is equivalent to a spherical averaging of the cross section for a single crystal for all $\vec{Q}$ having a given modulus $|\vec{Q}|$, and these vectors, when reduced to the first Brillouin zone, will give an approximate average over the entire zone if $|\vec{Q}|$ is sufficiently large.[69,70] In justifying the method for an amorphous solid, it has usually been pictured as a polycrystal,[71] but this is not necessary since one can argue more directly as follows.[72]

The one-phonon contribution to the cross section for the low spectrum in coherent inelastic scattering is proportional to[73]

$$\alpha(\vec{Q}, E) = \frac{n(E)-1}{E}\, e^{-W(\vec{Q})} \sum_n \delta(E_n - E) I_n(\vec{Q}) \,. \quad (11)$$

This is a sum over all vibrational eigenstates n. The factors entering this expression are a phonon occupation factor, a Debye-Waller factor,[72] a δ function expressing energy conservation, and a term which sums the contributions from all atoms j,

$$I_n(\vec{Q}) = \left| \sum_j \vec{u}_j^n \cdot \vec{Q}\, e^{i\vec{Q}\cdot\vec{R}_j} \right|^2 . \quad (12)$$

Here $\vec{R}_j$ denotes the position of the jth atom and $\vec{u}_j^n$ is its displacement vector for the nth vibrational eigenstate. In a random-network structure, one may argue that if Q is much greater than 2π times the inverse of the spread in nearest-neighbor distance, the phase $\vec{Q}\cdot\vec{R}_j$ is essentially random and (2) may be replaced by $\sum_j |\vec{u}_j \cdot \vec{Q}|^2$, which may in turn be replaced by $\frac{1}{3}|\vec{Q}|^2$ since the system is isotropic and $\sum_j |\vec{u}_j|^2$ is normalized to unity. Thus, in the high-Q limit, one expects the coherent inelastic-neutron spectrum to approach the phonon density of states $n(E)$. In practice, multiple-phonon processes become important at high Q; so some compromise is necessary.[35] Thus it is important to understand the effects of structural correlations on the form of the spectrum for intermediate values of Q.

Model calculations should be useful in the design and interpretation of neutron-energy-loss experiments. In order to apply (12) to our models, all we need to do is compute eigenvalues and eigenvectors and perform the indicated operations. We present results for periodic and quasiperiodic models and compare them with those expected for a polycrystalline powder of diamond-cubic material.

For the periodic model we regard the basic unit as a unit cell of an infinite crystal. In this case the usual crystal selection rules imply that Q must differ from the k vector of the modes which contribute by a multiple of a reciprocal-lattice vector. However, in the limit that the unit cell is very large, the Bragg points of the reciprocal lattice fill k space quite densely. Thus if we restrict attention to $\vec{k}=0$ modes of the 61-atom model, as we have done, we may still obtain $S(\vec{Q}, E)$ for a fairly dense grid of $\vec{Q}$ points. In Fig. 20 we show such results for $S'(\vec{Q}, E)$, which is $S(\vec{Q}, E)$ without the Debye-Waller and phonon occupation factors. Parameters appropriate to Ge have been used.

From the figure we see that at low Q there is a sound-wave-like peak at a frequency proportional to $|\vec{Q}|$. As $|\vec{Q}|$ increases, there is an oscillation of intensity between high- and low-frequency parts of the spectrum with a period of about 1.5 Å^{-1} su-

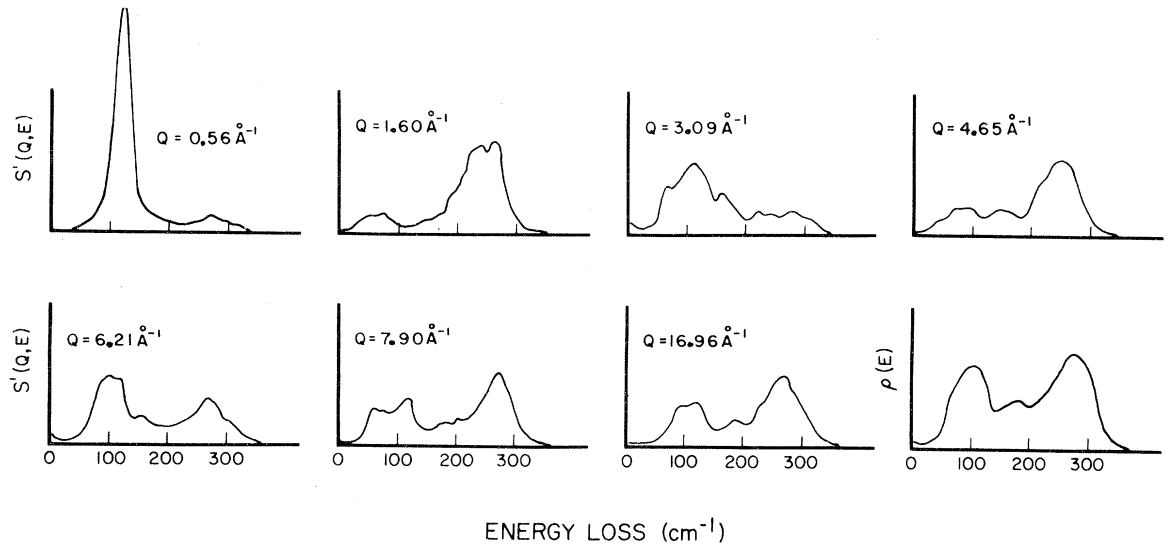

FIG. 20. Calculated neutron energy-loss spectra for different values of momentum transfer $\vec{Q}$ for the 61-atom network model. $S'(\vec{Q}, E)$ is related to the usual dynamic structure factor $S(\vec{Q}, E)$ as follows: $S'(\vec{Q}, E) = S(\vec{Q}, E)\{[n(\omega)+1]/\omega\} \times |\vec{Q}|^2)^{-1}$. The vibrational density of states $\rho(E)$ is shown for comparison. Parameters appropriate for Ge were used.

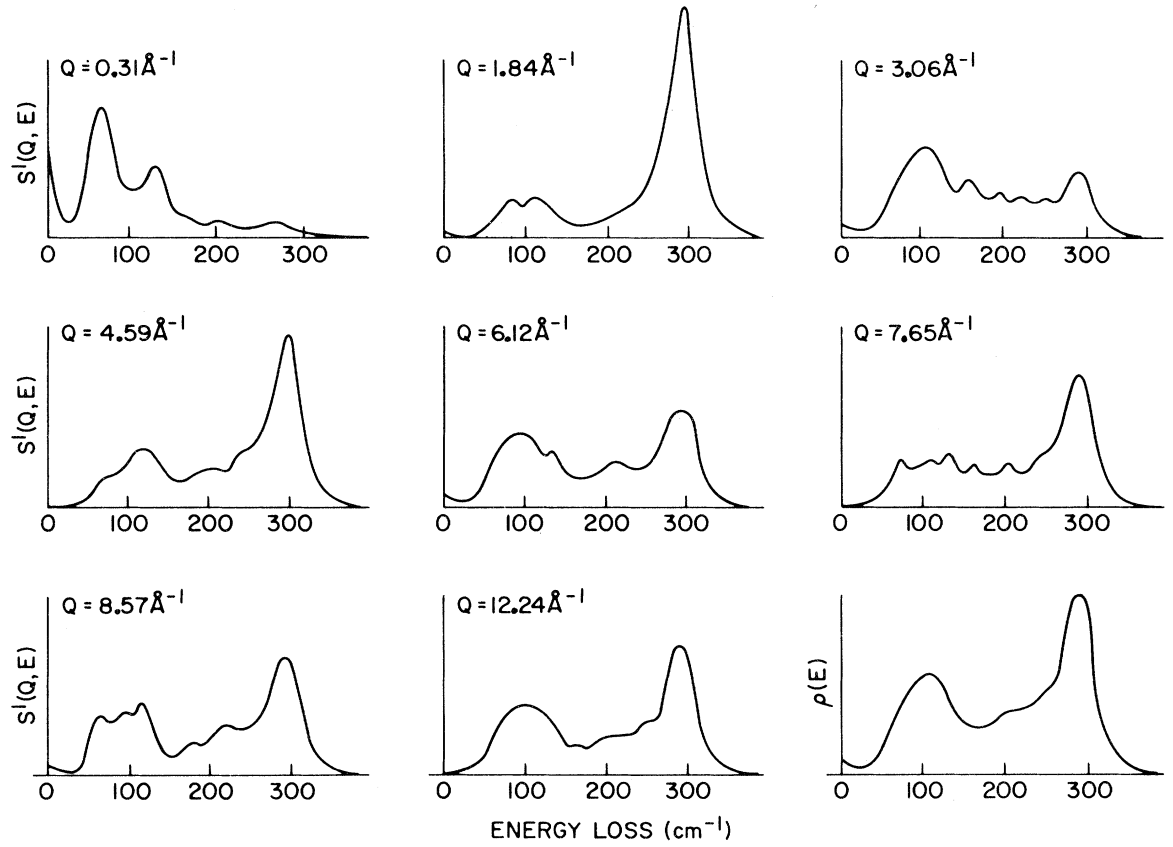

FIG. 21. Calculated neutron energy-loss spectra for the 85-atom quasiperiodic model for Ge (see also Fig. 20).

perimposed on a background proportional to the density of states. For $|\vec{Q}|$ greater than 6 Å^{-1}, the scattering is almost indistinguishable from the density of states.

In Fig. 21 we show similar results for an 85-atom quasiperiodic model. In this case the scattering is treated as being due to a finite cluster, and with this interpretation we may obtain meaningful results for any $\vec{Q}$. The results shown are for $\vec{Q}$'s along the z spatial axis. The results are similar to those for the periodic model. We have also considered $\vec{Q}$'s along the x direction and obtained similar results.

For comparison, we show in Fig. 22 results for scattering from a diamond-cubic polycrystalline powder. Except for the sharpness of the high-energy peaks in $S(\vec{Q}, E)$, which follows from the relative sharpness of this peak in the density of states, the behavior resembles that of the amorphous model's sound-wave-like behavior followed by intensity oscillations with increasing $|\vec{Q}|$, and eventually a spectrum proportional to the density of states. However, for the polycrystal the intensity oscillations are far more complex than the simple behavior seen in the results for the amorphous materials.

These results show that inelastic neutron scattering at sufficiently high $|\vec{Q}|$ (above about 8–9 Å^{-1}) or averaged over the oscillation period (1.5 Å^{-1}) should give a quite direct measure of the density of vibrational states in amorphous materials. They also indicate that oscillations in peak intensity with increasing $|\vec{Q}|$ are to be expected because of structural correlations implicit even in random structures. Figure 23 illustrates this oscillation of intensity between the TA and TO peaks. Here we plot the ratio of the intensity for the energy loss corresponding to the maximum in the upper peak of the density of states to that at the maximum in the lower peak. As $|\vec{Q}|$ increases the ratio (for two different directions of $\vec{Q}$) displays quantitatively the regular oscillations evident in Figs. 20 and 21. This oscillation agrees extremely well with a simple function derived (with no adjustable parameters) from the following approximations[72]: (i) Modes in these two peaks are given the exact "pure-bonding" or "pure-antibonding" character discussed in Sec. VI A, which arises from tetrahedral symmetry and the dominance of central forces. (ii) All other correlations are neglected. The function which gives the ratio of the weights of the lower and upper peaks is derived in Appendix C. With

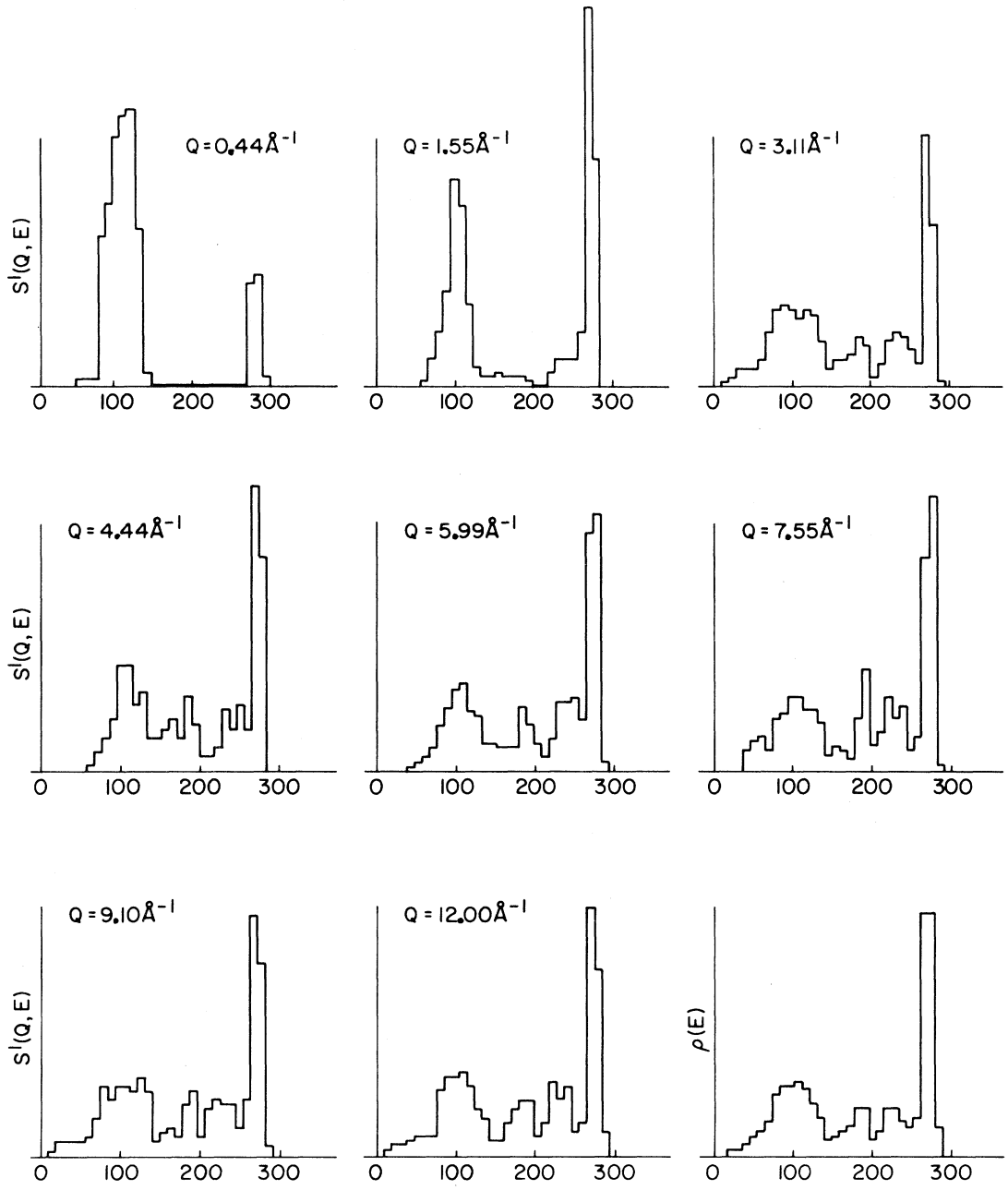

FIG. 22. Calculated neutron energy-loss spectra for a diamond cubic structure polycrystalline Ge powder. Histograms represent contributions of from 1000 to 3000 modes with $|\vec{k}+\vec{T}| = |\vec{Q}|$ within ± 0.22 Å^{-1} of the values indicated. ($\vec{T}$ is a reciprocal-lattice vector.)

the appropriate factor converting the ratio of weights to that of heights, this function is given in Fig. 23 by the full line. The agreement is seen to be excellent even for comparatively low values of $|\vec{Q}|$. We expect that this oscillation should be found in real materials. We might note, however, that for $|\vec{Q}| \geq 8$ Å^{-1}, the oscillation is sufficiently small that we would predict that the neutron energy loss does effectively reproduce the density of states. For a more accurate measure of the density of states, it appears that the loss spectrum should be averaged over one or more complete oscillations.

VII. CONCLUSIONS

As is the case with many electronic properties, the vibrational properties of Si and Ge are dominated by the effects of short-range order. For the

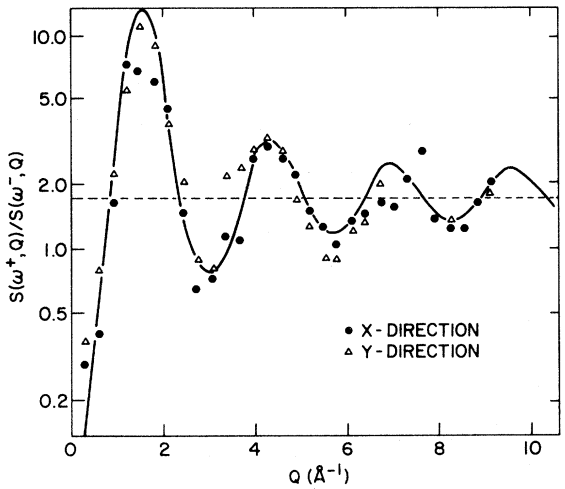

FIG. 23. Ratio of calculated neutron scattering cross sections for frequencies corresponding to the upper and lower density-of-states peaks for the 85-atom model compared to the calculated results for independently scattering bond contributions. The dashed line gives the ratio of the density-of-states peak heights. Full line is the theoretical result described in Appendix C. The frequencies ω^+ and ω^- are, respectively, 0.97 and 0.39 times the TO frequency of the diamond cubic structure of Ge.

amorphous phase, the broad features of the density of states and the variation with frequency of the matrix elements which weight the Raman and infrared spectra can be rather well explained in terms of such short-range order and the complete absence of any effects due to correlations of longer range ("$\vec{k}$-selection" effects). Approaches which start from results for perfect crystals and attempt to smear out spectra to the point where they agree with results for the amorphous phase are therefore in some difficulty. Even were they to succeed, we feel that they obscure the simplicity of the situation by including effects due to long-range correlations and then trying to dispel them by uncertain procedures!

While it is an interesting intellectual exercise to show that short-range order is, *per se*, sufficient to explain a great deal, it must be admitted that it would be highly desirable to go one stage further and achieve an understanding of the finer details of the spectrum and their relation to structure. This is, however, a difficult task, necessitating consideration of forces of longer range as well as the achievement of calculations for clusters of larger size. In the latter regard, the outlook is hardly encouraging, since a significant reduction in the "noise" due to the finite size of the clusters demands a high price in computer time and storage. For the present, we would caution against overinterpretation of the finer details of the numerical calculations performed so far.

The availability in the forseeable future of neutron-scattering data of high resolution should be of considerable assistance, since this will present a picture of the density of states which, while subject to various uncertainties, requires no subtraction of matrix-element effects.

ACKNOWLEDGMENTS

We wish to thank D. Henderson and D. E. Polk for providing the coordinates of their random-network modes and J. D. Axe, G. S. Cargill III, G. A. N. Connell, N. Shevchik, F. Stern, and M. F. Thorpe for helpful conversations.

APPENDIX A: INFRARED AND RAMAN MATRIX ELEMENTS

Consider the infrared absorption matrix element (5). This can be rearranged in a number of different ways, of which the one given below would appear to be the most illuminating and useful. Writing $C_\Delta(l)$ for the compression of the Δth bond associated with atom l, for a given vibrational eigenstate, $\vec{M}$ may be written

$$\vec{M} = 2\sum_l \left(\sum_\Delta C_\Delta(l)\right)\left(\sum_{\Delta'} \vec{r}_{\Delta'}(l)\right) . \tag{A1}$$

This may be obtained simply by multiplying out the expression (5), keeping the cross terms, and noting that the others cancel on each bond.

The second factor in the summand vanishes for exact tetrahedral symmetry, since then

$$\sum_\Delta \vec{r}_\Delta(l) = 0 . \tag{A2}$$

Thus the chosen mechanism is such that it gives *zero* for any structure with exact tetrahedral coordination of nearest neighbors,[73] and the total infrared intensity for random-network structures should scale roughly as the square of the distortion from tetrahedral symmetry, as given by mean-square value of $|\sum_\Delta \vec{r}_\Delta(l)|$.

There is, however, a remaining factor in the summand of (A1) which depends on the character of the vibrational eigenstate. Since it involves the compression of bonds, it might be expected to increase monotonically, roughly as was explained in Sec. VI B in connection with the Raman tensor. However, for the case of exact tetrahedral symmetry and central forces only, we know, in particular, that

$$\sum_\Delta C_\Delta(l) = 0 \tag{A3}$$

for the modes in the δ function at the top of the spectrum. This follows from the development of Sec. VI, since these modes are analogous to "pure-p-bonding" electronic wave functions; the contributions to the compression of each bond due to the

displacements of the two atoms at its end are equal. This, together with (A2), gives (A3).

Thus, in the absence of noncentral forces, the dipole associated with these particular modes should be of *second* order in the distortions (i.e., the intensity is of fourth order). As argued in the main text, the inclusion of the small noncentral forces should not alter this conclusion qualitatively. This therefore would appear to be a sufficient explanation of the relatively low infrared intensity associated with these modes in the calculations of Fig. 8.

Note that in the case of III-V compounds the dominant contribution to the infrared intensity is not of the form (A1), so the arguments given here are not applicable.

The Raman polarizability tensors $\overleftrightarrow{\alpha}_1$ [Eq. (6)] and $\overleftrightarrow{\alpha}_3$ [Eq. (8)] can also be written in terms of the $C_\Delta(l)$'s:

$$\overleftrightarrow{\alpha}_1 = \sum_{\text{bonds}} [\vec{r}_\Delta(l)\vec{r}_\Delta(l) - \tfrac{1}{3}\overleftrightarrow{1}]C_\Delta(l)\,, \tag{A4}$$

$$\overleftrightarrow{\alpha}_3 = \sum_{\text{bonds}} \overleftrightarrow{1}\, C_\Delta(l)\,, \tag{A5}$$

where each bond is counted only once in the sums. If the contributions from each bond add incoherently, then the Raman cross section from these mechanisms will be given by the mean-square value of $C_\Delta(l)$, i.e., the mean-square compression of the bonds. The latter has a simple frequency dependence in the case of central forces. The equation of motion for this case is

$$m\omega^2 \vec{u}_l = 3\alpha \sum_\Delta C_\Delta(l)\vec{r}_\Delta(l)\,. \tag{A6}$$

Taking the scalar product of both sides of (A6) with $\vec{u}_l$ and summing over all l, we obtain

$$m\omega^2 \sum_l u_l^2 = 3\alpha \sum_{\text{bonds}} [C_\Delta(l)]^2\,. \tag{A7}$$

When both sides are divided by the number of bonds, this equation shows that the mean-square bond compression is proportional to ω^2 times the mean-square displacement. The reduced Raman intensity per mode from mechanisms Nos. 1 and 3 is thus seen to vary as ω^2 over the whole spectrum in the case of central forces when correlations among different bonds are neglected.

APPENDIX B

In this appendix we give a proof of the theorem of Sec. VI A. As explained there, we introduce variables χ according to

$$\chi_\Delta(l) = (\sqrt{\tfrac{3}{4}})\vec{u}_l \cdot \vec{r}_\Delta(l)\,. \tag{B1}$$

With perfectly symmetric tetrahedral coordination of nearest neighbors they are related by

$$\sum_\Delta \chi_\Delta(l) = 0\,, \tag{B2}$$

since $\sum_\Delta \vec{r}_\Delta(l)$ is 0 for each l. The potential energy associated with nearest-neighbor central forces, given by Eq. (2), may be written

$$V = \frac{1}{2}\left(4\alpha \sum_{l\Delta} \chi_\Delta(l)^2 + 4\alpha \sum_{l\Delta} \chi_\Delta(l)\chi_\Delta(l\Delta)\right)\,. \tag{B3}$$

The kinetic energy may be written

$$T = \tfrac{1}{2} m \sum_{l\Delta} \dot{\chi}_\Delta(l)^2\,, \tag{B4}$$

since

$$\sum_\Delta \vec{r}_\Delta(l)\vec{r}_\Delta(l) = \tfrac{4}{3}\overleftrightarrow{1}\,. \tag{B5}$$

Now, the eigenvalues of the dynamical matrix derived by taking second derivatives of V with respect to the χ's would give the normal-mode frequencies (to be precise, $m\omega^2$) were it not for the linear dependence (B2) of the variables. To allow for this an extra term $\frac{1}{2}\lambda\sum_l [\sum_\Delta \chi_\Delta(l)]^2$ can be added to V and, in the limit $\lambda \to \infty$, that part of the spectrum which remains at finite frequencies is the required solution; i.e., the extra term projects out vectors which obey (B2). With this addition the problem is now identical to that studied by Thorpe and Weaire[60] in the context of electronic properties, provided we make the identifications

$$\begin{aligned} &m\omega^2 - 4\alpha \to E\,,\\ &4\alpha \to V_2\,,\\ &\lambda(\to\infty) \to V_1\,. \end{aligned} \tag{B6}$$

However, the spectrum of the tight-binding Hamiltonian of Thorpe and Weaire is in turn related to that of the simpler "one-band" Hamiltonian

$$H^{(1)} = V \sum_{l\Delta} |l\rangle\langle l\Delta|\,. \tag{B7}$$

Here there is just one basis function $|l\rangle$ associated with each site.

In the limit $V_1 \to \infty$, the eigenvalues of the full tight-binding Hamiltonian are related to those of (B6), denoted by ϵ, according to

$$E = -\tfrac{1}{4} V_2 V^{-1}\epsilon\,, \tag{B8}$$

apart from two δ functions at $E = \pm V_2$.[60] This translates, using (B6), into the theorem stated in Sec. VI.

APPENDIX C: COMPARISON OF TA AND TO MODES IN NEUTRON SPECTRUM

TA and TO modes are such that, approximately, the projections of the displacements of neighboring atoms onto their common bond are equal in magnitude and, respectively, of the same or opposite

sign. Furthermore, the factor $\vec{Q}\cdot\vec{u}_l$ which enters the neutron-scattering transition probability is approximately proportional to

$$\frac{3}{4}\sum_{\Delta}[\vec{Q}\cdot\vec{r}_{\Delta}(l)][\vec{u}_l\cdot\vec{r}_{\Delta}(l)]\,, \tag{C1}$$

since $\overleftrightarrow{I}=\frac{3}{4}\sum_{\Delta}\vec{r}_{\Delta}(l)\vec{r}_{\Delta}(l)$ for tetrahedral symmetry ($\overleftrightarrow{I}$ is the unit dyadic). Using this we can write the scattering amplitude, i.e., the expression whose absolute square gives the intensity in (13), as a sum over bonds. The contribution of one bond connecting two atoms A and B to the amplitude for a particular TO or TA mode is

$$\begin{aligned} a_{AB}^{\mathrm{TO}} &= \tfrac{3}{4}e^{i\vec{Q}\cdot\vec{R}_0^{AB}}\vec{Q}\cdot\Delta\vec{R}^{AB}\sin\tfrac{1}{2}\vec{Q}\cdot\Delta\vec{R}^{AB}U_{-}^{AB}\,, \\ a_{AB}^{\mathrm{TA}} &= \tfrac{3}{4}e^{i\vec{Q}\cdot\vec{R}_0^{AB}}\vec{Q}\cdot\Delta\vec{R}^{AB}\cos\tfrac{1}{2}\vec{Q}\cdot\Delta\vec{R}^{AB}U_{+}^{AB}\,, \end{aligned} \tag{C2}$$

where $\vec{R}_0^{AB}$ is the center of the AB bond, $\Delta\vec{R}_0^{AB}$ is the vector from atom A to atom B, and $U_{\pm}^{AB}$ is $(\vec{U}_A \pm \vec{U}_B)\cdot\vec{r}_{AB}$. We assume that the phase of the U^{AB} together with the factor $e^{i\vec{Q}\cdot\vec{R}_0^{AB}}$, varies sufficiently randomly from one bond to the next to justify the "incoherent approximation," which gives for the intensities

$$I^{\mathrm{TO}}\propto\sum_{\text{bonds}}(a^{\mathrm{TO}})^2\,,\quad I^{\mathrm{TA}}\propto\sum_{\text{bonds}}(a^{\mathrm{TA}})^2\,. \tag{C3}$$

With such an approximation, a simple spherical average gives

$$\begin{aligned} I^{\mathrm{TO}} &\propto \int_0^{\pi}(QR\cos\theta)^2\sin^2(\tfrac{1}{2}QR\cos\theta)\sin\theta\,d\theta\,, \\ I^{\mathrm{TA}} &\propto \int_0^{\pi}(QR\cos\theta)^2\cos^2(\tfrac{1}{2}QR\cos\theta)\sin\theta\,d\theta\,, \end{aligned} \tag{C4}$$

since the system is assumed to be (macroscopically) isotropic and there are no preferred directions for the bonds. R is the magnitude of the nearest-neighbor distance, taken to be constant. Equation (B4) may be rewritten

$$\begin{aligned} I^{\mathrm{TO}} &\propto \frac{4}{QR}\int_{-QR/2}^{QR/2}\mu^2\sin^2\mu\,d\mu\,, \\ I^{\mathrm{TA}} &\propto \frac{4}{QR}\int_{-QR/2}^{QR/2}\mu^2\cos^2\mu\,d\mu\,. \end{aligned} \tag{C5}$$

The ratio of the intensities of the two types of modes is

$$\begin{aligned} \frac{I_{\mathrm{TO}}}{I_{\mathrm{TA}}} &= \int_0^{QR/2}\mu\sin^2\mu\,d\mu\Big/\int_0^{QR/2}\mu^2\cos^2\mu\,d\mu \\ &= \frac{\frac{1}{2}-\frac{3}{2}(QR)^{-1}\sin QR-3(QR)^{-2}\cos QR+3(QR)^{-3}\sin QR}{\frac{1}{2}+\frac{3}{2}(QR)^{-1}\sin QR+3(QR)^{-2}\cos QR-3(QR)^{-3}\sin QR}\,. \end{aligned} \tag{C6}$$

This has the asymptotic behavior

$$I_{\mathrm{TO}}/I_{\mathrm{TA}}\sim 1-6(QR)^{-1}\sin QR\,,\quad \text{as } Q\to\infty \tag{C7}$$

in keeping with the assertion that the spectrum should represent the density of states in this limit.

Note also that the sum rule

$$I_{\mathrm{TA}}+I_{\mathrm{TO}}=(\text{const})Q^2 \tag{C8}$$

also follows from (C5); so the combined contribution to the spectrum from the lowest and highest peaks is constant in this approximation. There is also a sum rule on the whole spectrum.[73]

---

†Supported in part by NSF Grant No. GH 3599 and U. S. AFOSR Contract No. F44620-71-C-0039.

[1]R. Temkin, G. N. Connell, and W. Paul, Adv. Phys. 22, 581 (1974).
[2]D. E. Polk, J Non-Cryst. Solids 5, 365 (1971).
[3]M. L. Rudee and A. Howie, Philos. Mag. 25, 1001 (1972).
[4]D. Henderson, in *Computational Solid State Physics*, edited by F. Herman (Plenum, New York, 1972), p. 175.
[5]F. D. Bundy and J. S. Kasper, Science 139, 340 (1963).
[6]R. Alben, S. Goldstein, M. F. Thorpe, and D. Weaire, Phys. Status Solidi 53, 545 (1972).
[7]J. D. Joannopoulos and M. L. Cohen, Phys. Rev. 7, 2644 (1973).
[8]I. B. Ortenburger and D. Henderson, in *Proceedings of the Eleventh International Conference on the Physics of Semiconductors, Warsaw* (Polish Scientific Publishers, Warsaw), p. 465.
[9]R. J. Kobliska, S. A. Solin, M. Selders, R. K. Chang, R. Alben, M. F. Thorpe, and D. Weaire, Phys. Rev. Lett. 29, 725 (1972).
[10]J. S. Kasper, P. Hagenmuller, M. Pouchard, and C. Cros, Science 150, 1713 (1965).
[11]R. J. Bell, Rep. Prog. Phys. 35, 1315 (1972).
[12]P. Dean, Rev. Mod. Phys. 44, 127 (1972).
[13]G. Lucovsky, in *Amorphous and Liquid Semiconductors*, edited by J. Stuke and W. Brenig (Taylor and Francis, London, 1974), p. 1099.
[14]H. Böttger, Phys. Status Solidi B 62, 9 (1974).
[15]J. E. Smith, Jr., M. H. Brodsky, B. L. Crowder, and M. I. Nathan, in *Proceedings of the Second International Conference on Light Scattering in Solids*, edited by M. Balkanski (Flammarion, Paris, 1971), p. 330.
[16]P. H. Gaskell, Disc. Faraday Soc. 50, 82 (1970).
[17]M. F. Thorpe, in Ref. 13, p. 835.
[18]R. Shuker and R. W. Gammon, Phys. Rev. Lett. 25, 222 (1970).
[19]E. Walley and J. E. Bertie, J. Chem. Phys. 46, 1264 (1966).
[20]M. Hass, J. Phys. Chem. Solids 31, 415 (1970).
[21](a) J. E. Smith, Jr., M. H. Brodsky, B. L. Crowder, M. I. Nathan, and A. Pinczuk, Phys. Rev. Lett. 26, 642 (1971). (b) *HH* refers to horizontal polarization of both the incident and scattered beam, *HV* refers to horizontal and vertical polarizations, respectively. The depolarization ratio is the ratio of *HV*:*HH* contributions.
[22]J. E. Smith, Jr., M. H. Brodsky, B. L. Crowder, and M. I. Nathan, J. Non-Cryst. Solids 8-10, 179 (1972).
[23]B. L. Crowder, J. E. Smith, Jr., M. H. Brodsky,

and M. I. Nathan, in *Proceedings of the International Conference on Ion Implantation*, Garmisch, 1971.
[24]M. Wihl, M. Cardona, and J. Tauc, J. Non-Cryst. Solids 8-10, 172 (1972).
[25]J. S. Lannin, Solid State Commun. 11, 1523 (1972).
[26]J. S. Lannin, Solid State Commun. 12, 947 (1973).
[27]J. Tauc, A. Abraham, R. Zallen, and M. Slade, J. Non-cryst. Solids 4, 279 (1970).
[28]W. Prettl, N. J. Shevchik, and M. Cardona, Phys. Status Solidi B 59, 241 (1973).
[29]M. H. Brodsky and A. Lurio, Phys. Rev. B 9, 1646 (1974).
[30](a)R. W. Stimets, J. Waldman, J. Lin, T. S. Chang, R. J. Temkin, and G. A. N. Connell, Solid State Commun. 13, 1485 (1973); (b) J. R. Hendrickson, U. Strom, P. C. Taylor, and S. K. Bahl, in *Tetrahedrally Bonded Amorphous Semiconductors*, edited by M. H. Brodsky, S. Kirkpatrick, and D. Weaire (AIP, New York, 1974), p. 290.
[31]F. R. Ladan and A. Zylberstejn, Phys. Rev. Lett. 29, 1198 (1973).
[32]F. R. Ladan, thesis (University of Paris VI, 1972) (unpublished).
[33]B. Schröder and J. Geiger, Phys. Rev. Lett. 28, 301 (1972).
[34]B. Schröder, in *Tetrahedrally Bonded Amorphous Semiconductors*, edited by M. H. Brodsky, S. Kirkpatrick, and D. Weaire (AIP, New York, 1974), p. 114.
[35](a) J. D. Axe, D. T. Keating, G. S. Cargill III, and R. Alben, in Ref. 34, p. 279; (b) G. Dolling and R. A. Cowley, Proc. Phys. Soc. Lond. 88, 463 (1966).
[36]R. J. Kobliska and S. A. Solin, in Ref. 8, p. 477.
[37]R. J. Kobliska and S. A. Solin, Phys. Rev. B 8, 3799 (1973).
[38]P. Steinhardt, R. Alben, and D. Weaire, J. Non-cryst. Solids 15, 199 (1974).
[39]M. G. Duffy, D. S. Boudreaux, and D. E. Polk, J. Non-cryst. Solids 15, 435 (1974).
[40]L. Gultman, in Ref. 34, p. 225.
[41]P. N. Keating, Phys. Rev. 145, 637 (1966).
[42]G. Nelin and G. Nilsson, Phys. Rev. B 5, 3151 (1972).
[43]F. Herman, J. Phys. Chem. Solids 8, 405 (1959).
[44]Strictly speaking, this is only correct for those structures in which the bond lengths are all equal. There is some arbitrariness in the adaptation of Keating's formulation to random networks.
[45]B. D. Singh and B. Dayal, Phys. Status Solidi 38, 141 (1970).
[46]M. Born, Ann. Phys. (Leipz.) 44 605 (1914).
[47]See, e.g., Ref. 41.
[48]R. M. Martin, Phys. Rev. 1, 4005 (1970).
[49]G. Dolling and R. A. Cowley, Proc. Phys. Soc. Lond. 88, 463 (1966).
[50]J. C. Phillips, *Bonds and Bands in Semiconductors* (Academic, New York, 1974).
[51]R. Loudon, Adv. Phys. 13, 423 (1964).
[52]M. Lax and E. Burstein, Phys. Rev. 97, 39 (1955).
[53]L. R. Swanson and A. A. Maradudin, Phys. Rev. 2, 3891 (1970).
[54]M. Lax, Phys. Rev. Lett. 1, 131 (1958); 1, 133 (1958).
[55]R. Zallen, Phys. Rev. 173, 824 (1968).
[56]I. Chen and R. Zallen, Phys. Rev. 173, 833 (1968).
[57]Similar theorems can be developed for other types of local symmetry. In particular, a system with symmetric threefold bonding in two dimensions will obey a theorem of this type. The only lattice which *strictly* obeys this condition is the honeycomb lattice, whose degenerate eigenstates at zero and finite frequencies are rather well known.
[58]D. Weaire and R. Alben, Phys. Rev. Lett. 29, 1505 (1972).
[59]R. Alben, D. Weaire, J. E. Smith, Jr., and M. Brodsky, in *Proceedings of the Fifth International Conference on Amphorous and Liquid Semiconductors*, Garmisch, 1973 (Taylor and Francis, London 1974), p. 1231.
[60]M. F. Thorpe and D. Weaire, Phys. Rev. B 4, 3518 (1971).
[61]M. F. Thorpe, J. Math. Phys. 13, 294 (1972).
[62]M. F. Thorpe and D. Weaire, Phys. Rev. Lett. 27, 1581 (1971).
[63]G. Wiech and E. Zöph, in *Proceedings of the International Conference on Band Structure Spectroscopy of Metals and Alloys*, Glasgow, 1971, edited by D. J. Fabian and L. M. Watson (Academic, London, 1973) p. 629.
[64]L. Ley, S. Kowalczyk, R. Pollak, and D. A. Shirley, Phys. Rev. Lett. 29, 1088 (1972).
[65]W. D. Grobman and D. E. Eastman, Phys. Rev. Lett. 29, 1508 (1972).
[66]R. Alben and D. Weaire, J. Phys. C 6, L384 (1973).
[67]Special arguments can be made regarding the low-frequency regime (Ref. 19) leading to an expected variation of Raman activity as ω^2. While less approximate than the remarks made in the text, which apply to the whole spectrum, these arguments are not entirely rigorous. Experiment supports an ω^2 variation (Ref. 26). In the case of the infrared spectrum, Prettl *et al.* (Ref. 28) have argued in favor of an ω^4 dependence; the derivation of this is less certain.
[68]J. D. Axe (unpublished).
[69]I. P. Eremeev, I. P. Sadikov, and A. A. Chernyshov, Fiz. Tverd. Tela 15, 1953 (1973) [Sov. Phys–Solid State 15, 1309 (1974)].
[70]F. W. DeWette and A. Rahman, Phys. Rev. 176, 784 (1968).
[71]A. J. Leadbetter, A. C. Wright, and A. J. Apling, in *Amorphous Materials*, edited by R. W. Douglas and B. Ellis (Wiley, New York, 1972), p. 423.
[72]D. Weaire and R. Alben, J. Phys. C 7, L189 (1974).
[73]W. M. Lomer and G. G. Low, in *Thermal Neutron Scattering*, edited by P. A. Egelstaff (Academic, London, 1965), p. 1.